Automatica 138 (2022) 110137

Contents lists available at ScienceDirect

Automatica

journal homepage: www.elsevier.com/locate/automatica

Delay-compensated event-triggered boundary control of hyperbolic PDEs for deep-sea construction☆

Ji Wang [a,*], Miroslav Krstic [b]

[a] Department of Automation, Xiamen University, Xiamen 361005, China
[b] Department of Mechanical and Aerospace Engineering, University of California, San Diego, La Jolla, CA 92093-0411, USA

ARTICLE INFO

Article history:
Received 28 March 2021
Received in revised form 5 August 2021
Accepted 19 November 2021
Available online 18 January 2022

Keywords:
Distributed parameter system
Delay
Boundary control
Event-triggered control
Deep-sea construction

ABSTRACT

In this paper, we present delay-compensated event-triggered boundary control of heterodirectional coupled hyperbolic PDE–ODE systems, with the purpose of employing a piecewise-constant control input which makes the control law more user-friendly in deep-sea construction vessels where the actuator, i.e., the ship-mounted crane, is massive, and compensating delays that exist in transmission of sensing signals from the seabed to the vessel on the ocean surface through a set of acoustics devices. After treating the time delay of arbitrary length as a transport PDE whose boundary connects with the plant, a state observer is built to estimate the states of the overall system of heterodirectional coupled hyperbolic PDEs–ODE–transport PDE, only using the measurements at the right boundary of the last transport PDE. An observer-based output-feedback continuous-in-time controller is designed to stabilize the overall system using the backstepping method, followed by an observer-based event-triggering mechanism, which is designed based on the evolution of the overall PDE–ODE–PDE system, to determine the updating times of the actuation signal. The absence of a Zeno behavior and exponential convergence in the event-based closed-loop system are proved. In the simulation, the obtained theoretical result is verified in control of a deep-sea construction vessel to place the equipment in the target area on the seabed. Performance deterioration under extreme and unmodeled disturbances is also illustrated.

1. Introduction

1.1. Motivation

The motivation of this work arises from the control problem for a deep-sea construction vessel (DCV), which is used to place underwater parts of an off-shore oil drilling platform at the designated locations on the seabed (Stensgaard, White, & Schiffer, 2010), and is also used in the construction of artificial reefs for enabling the development and growth of marine life, in laying communication cables on the seabed, which is often uneven and rife with obstacles, and in other undersea applications. A diagram of DCV is shown in Fig. 1, where the top of a cable is attached to a crane on a vessel at the ocean surface and the cable's bottom is attached to an object to be installed/moved on the seabed (How, Ge, & Choo, 2010, 2011; Wang & Krstic, 2021d). Large oscillations often appear in the cable system, especially under the external ocean disturbances (How et al., 2010). The large oscillations would cause large deviation of the payload from the designated location on the seabed.

Several boundary control schemes have been proposed for the PDE-modeled cable systems with the purpose of suppressing the cable oscillations (He & Ge, 2016; He, Meng, He, & Ge, 2018; Wang, Koga, Pi and Krstic, 2018). In addition to the infinite-dimension property introduced by the cable structure, there are two challenges in the control design of DCV. The first one is the existence of sensor delays. As shown in Fig. 1, the sensor signal measured at the payload is transmitted over a large distance to the vessel on the ocean surface through a set of acoustics devices, because acoustic communication is the most versatile and widely used technique in underwater engineering applications considering low attenuation in water (Jiang, 2008; Manjula & Manvi, 2011). The transmission speed of acoustic signals in salty water is around 1500 m/s, which is a difference of five orders of magnitude lower than the speed of electromagnetic wave in free space (Jiang, 2008). As a result, signal propagation delay in underwater becomes significant (Jiang, 2008). Such sensor signal delay may result in information distortion or even make the control system lose stability, which motivates us to study the delay

☆ The material in this paper was not presented at any conference. This paper was recommended for publication in revised form by Associate Editor Angelo Alessandri under the direction of Editor Thomas Parisini.

* Corresponding author.
E-mail addresses: jiwang@xmu.edu.cn (J. Wang), krstic@ucsd.edu (M. Krstic).

https://doi.org/10.1016/j.automatica.2021.110137
0005-1098/

compensation in the control design of DCV. The second one is that the massive actuator, i.e., the ship-mounted crane shown in Fig. 1, is incapable of supporting the fast-changing control signal, due to its low natural frequency, which motivates us to consider applying sampling schemes into the continuous-in-time control signals to reduce the changes in the actuation. Compared with the periodic sampled-data control where unnecessary movements of the massive actuator may appear, event-triggered control is more feasible from the point of view of energy saving, because the massive actuator is only animated at the necessary times which are determined by an event-triggering mechanism of evaluating the operation of the DCV.

In this paper, we pursue a delay-compensated event-triggered control scheme, which compensates the sensor delay of arbitrary length, and has a reduction of the changes in the actuator signal, i.e., the control input employs piecewise-constant values. The delay-compensated event-triggered control scheme is designed for a 2×2 hyperbolic PDE–ODE system, which not only covers the DCV dynamics, and can be suitable in some other applications, such as road traffic (Goatin, 2006; Yu & Krstic, 2019), water level dynamics (Diagne, Diagne, Tang, & Krstic, 2017; Prieur & Winkin, 2018), and flow of fluids in transmission lines (Hasan, Aama, & Krstic, 2016). The classical control results of the class of coupled hyperbolic PDEs are presented in Coron, Vazquez, Krstic, and Bastin (2013), Hu, Di Meglio, Vazquez, and Krstic (2016) and Vazquez, Krstic, and Coron (2011), which are further developed for the case including couplings with ODEs in Deutscher, Gehring, and Kern (2018), Meglio, Lamare, and Aarsnes (2020), Saba, Bribiesca-Argomedo, Loreto, and Eberard (2019) and Wang, Krstic and Pi (2018).

1.2. Event-triggered control of PDEs

Most of the current designs on event-triggering mechanisms are for ODE systems, such as Girard (2015), Heemels, Johansson, and Tabuada (2012), Marchand, Durand, and Castellanos (2013), Seuret, Prieur, and Marchand (2014) and Tabuada (2007). There exist some results on distributed (in-domain) control of PDEs, such as Selivanov and Fridman (2016) and Yao and El-Farra (2013). For boundary control, event-triggered control designs for reaction–diffusion PDEs were proposed in Espitia, Karafyllis, and Krstic (2021) and Karafyllis, Espitia, and Krstic (2021), and the results for first-order hyperbolic PDEs were presented in Diagne and Karafyllis (2021) and Espitia, Girard, Marchand, and Prieur (2016a, 2016b). Regarding the 2×2 first-order hyperbolic PDE, the first attempt of event-based boundary control was Espitia, Girard, Marchand, and Prieur (2018), which is in the state-feedback form. Based on the observer design, the output-feedback event-triggered boundary controllers of the 2×2 first-order hyperbolic PDEs were proposed in Espitia (2020) and Wang and Krstic (2022), and an adaptive event-triggered boundary controller is further developed in Wang and Krstic (2021a). However, a large delay is not allowed in the above event-triggered control designs.

1.3. Delay compensation/robustness in PDEs

Recently, regarding taking into consideration time delay, boundary control designs for hyperbolic PDEs have been proposed. For example, delay-robust stabilizing feedback control designs for coupled first-order hyperbolic PDEs were introduced in Auriol, Aarsnes, Martin and Di Meglio (2018) and Auriol, Bribiesca-Argomedo, Saba, Di Loreto and Di Meglio (2018), achieving robustness to small delays in actuation. In order to compensate arbitrarily long delays, a delay compensation technique was developed in Krstic (2009b) and Krstic and Smyshlyaev (2008), where the delay was captured as a transport PDE and the original

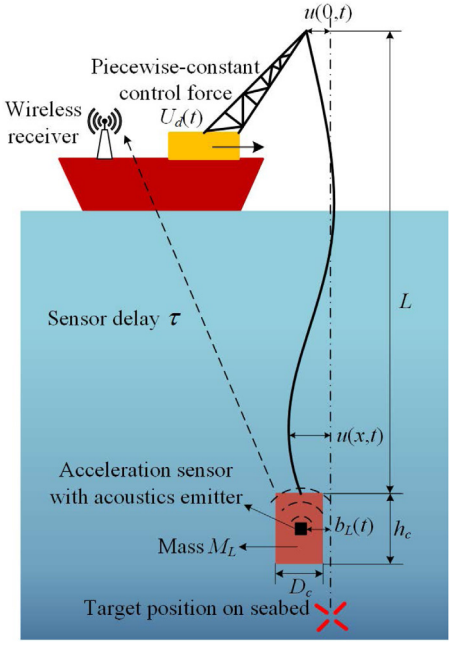

Fig. 1. Diagram of a deep-sea construction vessel.

ODE plant with sensor delay was treated as an ODE-transport PDE cascade in the controller and observer designs. Therein, the observer was built of a "full-order" type, which estimates both the plant states and the sensor states, compared with some classical results about delay-compensated observer designs (Ahmed-Ali, Karafyllis, & Lamnabhi-Lagarrigue, 2013; Cacace, Germani, & Manes, 2010; Germani, Manes, & Pepe, 2002), which only estimate plant states, namely, observers of the "reduced-order" type. While compensation of arbitrarily long delays by this technique is commonly available for finite-dimensional systems, only very few examples exist for PDEs, where the result for coupled first-order hyperbolic PDEs was presented in Wang and Krstic (2020a), and the results for parabolic (reaction–diffusion) PDEs were proposed in Koga, Bresch-Pietri, and Krstic (2020) and Krstic (2009a). Delay compensation for the wave PDEs with arbitrarily long delays is more complex than the one for reaction–diffusion PDEs, for which the primary reason is the second-order-in-time character of the wave equation. In Krstic (2011), by treating the delay as a transport PDE and applying the backstepping method, a boundary controller was designed for a wave PDE with a compensation of an arbitrarily long input delay and with a guarantee of exponential stability in the closed-loop system. Through truncation of the original infinite dimensional system and applying predictor feedback, control designs for PDEs with long input delays were also presented in Guzman, Marx, and Cerpa (2019), Lhachemi and Prieur (2020), Lhachemi, Prieur, and Shorten (2019) and Prieur and Trelat (2018). All the above delay compensation/robustness results employ the continuous-in-time control input, instead of a piecewise-constant fashion.

1.4. Main contributions

- Compared with the results in Espitia (2020), Espitia et al. (2018, 2021) and Wang and Krstic (2022) about event-triggered control of PDEs without delay compensation, we achieve compensation of arbitrarily long sensor delays in event-triggered control of hyperbolic PDE–ODE systems.

- The previous results (Koga et al., 2020; Krstic, 2009a, 2011; Wang & Krstic, 2020a) on delay-compensated control of PDEs use continuous-in-time control input signals, whereas the control input in this paper is piecewise constant.
- In comparison to the previous continuous-in-time controllers for DCVs without delay compensation (How et al., 2010, 2011; Wang & Krstic, 2021d), this paper develops a DCV control scheme, which compensates the sensor delays arising from the long-distance transmission of the sensing signal via acoustics devices, and employs a more user-friendly piecewise-constant actuation for the massive ship-mounted crane.

1.5. Organization

The DCV model, and the general model used in control design are presented in Section 2. Observer design is proposed in Section 3, where the observer gains are determined in two transformations which convert the observer error system to a target observer error system whose exponential stability is straightforward to obtain. An observer-based output-feedback continuous-in-time controller with delay compensation is designed in Section 4 by using the backstepping method. In Section 5, a dynamic event-triggering mechanism is designed, and the existence of a minimal dwell-time between two successive triggering times is proved. The absence of a Zeno behavior and exponential convergence in the event-based closed-loop system are proved in Section 6. The obtained theoretical result is verified in the application of DCV control for seabed installation by simulation in Section 7. The conclusions and future work are provided in Section 8.

1.6. Notation

We adopt the following notation.

- The symbol $\mathbb{R}_-$ denotes the set of negative real numbers, whose complement of the real axis is $\mathbb{R}_+ := [0, +\infty)$. The symbol $\mathbb{Z}_+$ denotes the set of all non-negative integers.
- Let $U \subseteq \mathbb{R}^n$ be a set with non-empty interior and let $\Omega \subseteq \mathbb{R}$ be a set. By $C^0(U; \Omega)$, we denote the class of continuous mappings on U, which take values in Ω. By $C^k(U; \Omega)$, where $k \geq 1$, we denote the class of continuous functions on U, which have continuous derivatives of order k on U and take values in Ω.
- We use the notation $L^2(0, 1)$ for the standard space of the equivalence class of square-integrable, measurable functions defined on $(0, 1)$ and $\|f\| = \left(\int_0^1 f(x)^2 dx\right)^{\frac{1}{2}} < +\infty$ for $f \in L^2(0, 1)$.
- For an $I \subseteq \mathbb{R}_+$, the space $C^0(I; L^2(0, 1))$ is the space of continuous mappings $I \ni t \mapsto u[t] \in L^2(0, 1)$.
- Let $u : \mathbb{R}_+ \times [0, 1] \to \mathbb{R}$ be given. We use the notation $u[t]$ to denote the profile of u at certain $t \geq 0$, i.e., $(u[t])(x) = u(x, t)$, for all $x \in [0, 1]$.

2. Problem formulation

2.1. Model of DCV

We follow the modeling process in Section 2 in Wang and Krstic (2021d) but make the following three simplifications: (1) We take the cable length as constant, i.e., we set $l(t)$ as L; (2) The spatially-dependent static tension of the cable, which considers the effect of the cable mass on the tension in the cable, is assumed as a constant static tension resulting from the payload mass and buoyancy, i.e., we set $T(x)$ as T_0; (3) We only focus on lateral vibrations instead of longitudinal–lateral coupled vibrations, and model the dynamics of a deep sea construction vessel as

$$T_0 u_{\bar{x}}(0, t) = U(t), \tag{1}$$

$$\rho u_{tt}(\bar{x}, t) = T_0 u_{\bar{x}\bar{x}}(\bar{x}, t) - d_c u_t(\bar{x}, t), \tag{2}$$

$$u(L, t) = b_L(t), \tag{3}$$

$$M_L \ddot{b}_L(t) = -d_L \dot{b}_L(t) + T_0 u_{\bar{x}}(L, t), \tag{4}$$

$\forall (\bar{x}, t) \in [0, L] \times [0, \infty)$. Eq. (2) describes the oscillation dynamics of the cable, where $u(\bar{x}, t)$ denotes the distributed transverse displacement along the cable. Eq. (4) models the dynamics of the payload, and the function $b_L(t)$ denotes its transverse displacement. Eq. (3) represents the connection between the bottom of the cable and the payload, and Eq. (1) describes the force input at the top of the cable, i.e., at the ship-mounted crane, where the control force $U(t)$ is to be designed in this paper. The static tension T_0 is defined as $T_0 = M_L g - F_{buoyant}$, where the buoyancy F_{buoyant} is $F_{\text{buoyant}} = \frac{1}{4}\pi D_c^2 h_c \rho_s g$. The physical parameters of the deep-sea construction vessel are given in Table 1, whose values are taken from How et al. (2011).

Table 1
Physical parameters of the DCV.

Parameters (units)	Values
Cable length L (m)	1000
Cable diameter R_d (m)	0.2
Cable linear density ρ (kg/m)	8.02
Payload mass M_L (kg)	4.0×10^5
Gravitational acceleration g (m/s^2)	9.8
Cable material damping coefficient d_c (N s/m)	0.5
Height of payload modeled as a cylinder h_c (m)	10
Diameter of payload modeled as a cylinder D_c (m)	5
Damping coefficient at payload d_L (N s/m)	2.0×10^5
Seawater density ρ_s (kg m^{-3})	1024

An accelerometer is placed at the object at the bottom of the cable, referred to as payload, to measure the lateral acceleration $\ddot{b}_L(t)$ of the payload. However, as shown in Fig. 1, there exists a sensor delay τ due to the fact that the sensor signal is transmitted over a large distance from the seabed to the vessel on the ocean surface through a set of acoustics devices, i.e., the acquisition of the wireless receiver at the vessel is the delayed measurement of the lateral acceleration of the payload, denoted as

$$y_{\text{out}}(t) = \dot{\zeta}(t - \tau), \quad t \in [\tau, \infty), \tag{5}$$

where a new variable is introduced as

$$\zeta(t) = \dot{b}_L(t). \tag{6}$$

In practice, the lateral velocity ζ of the payload is obtained by integrating the delayed acceleration sensing $y_{\text{out}}(t)$, i.e.,

$$\zeta(t - \tau) = \int_\tau^t y_{\text{out}}(h)dh + \zeta(0), \quad t \in [\tau, \infty), \tag{7}$$

which is a delayed signal of the lateral velocity, where the initial value $\zeta(0)$ of the lateral velocity at the payload can be calculated via (4), i.e., $\zeta(0) = \frac{-M_L}{d_L}\ddot{b}_L(0) + \frac{T_0}{d_L}u_{\bar{x}}(L, 0) = \frac{-M_L}{d_L}y_{\text{out}}(\tau) + \frac{T_0}{d_L}y_s(\tau)$, where y_{out} is given in (5), and $y_s(t) = u_{\bar{x}}(L, t - \tau)$ is the delayed signal obtained by a strain sensor placed at the connection point between the payload and the cable. Eq. (7) only explains an acquisition method for ζ in practical DCVs, and no restrictions are imposed on any initial conditions in the design and theory in this paper.

In the practical DCV, caused by ocean current, there always exist a distributed oscillating drag force $f(\bar{x}, t)$ along the cable and a drag force $f_L(t)$ at the payload, i.e., disturbances $f(\bar{x}, t), f_L(t)$

would exist in (2), (4). Although we do not deal with the disturbances $f(\bar{x},t), f_L(t)$ in the control design in this paper, they are considered in the simulation model for testing robust of the proposed controller.

2.2. Representing the model in Riemann coordinate

Applying the Riemann transformations (Wang & Krstic, 2021d)

$$\bar{z}(\bar{x},t) = u_t(\bar{x},t) - \sqrt{\frac{T_0}{\rho}}u_{\bar{x}}(\bar{x},t), \tag{8}$$

$$\bar{w}(\bar{x},t) = u_t(\bar{x},t) + \sqrt{\frac{T_0}{\rho}}u_{\bar{x}}(\bar{x},t), \tag{9}$$

introducing a space normalization variable

$$x = \frac{\bar{x}}{L} \in [0,1], \tag{10}$$

and defining

$$\bar{z}(\bar{x},t) = z(x,t), \quad \bar{w}(\bar{x},t) = w(x,t), \tag{11}$$

Eqs. (1)–(4) are rewritten as the plant (14)–(18) shown shortly, with the coefficients

$$\bar{c} = 2\sqrt{\frac{1}{T_0\rho}}, \quad q_1 = q_2 = \frac{1}{L}\sqrt{\frac{T_0}{\rho}}, \quad g_1 = g_2 = g_3 = g_4 = \frac{d_c}{2\rho}, \tag{12}$$

$$q = -1, \ p = 1, \ c = 2, \ a_1 = \frac{-d_L}{M_L} + \frac{\sqrt{T_0\rho}}{M_L}, \ b_1 = \frac{\sqrt{T_0\rho}}{M_L}, \tag{13}$$

where $\bar{z}_{\bar{x}}(\bar{x},t) = \frac{1}{L}z_x(x,t)$, $\bar{w}_{\bar{x}}(\bar{x},t) = \frac{1}{L}w_x(x,t)$ have been used.

2.3. General model

The plant considered in this paper is a general form of the model obtained from applying Riemann transformations (8), (9) into (1)–(4), and employing (10), (11), given by

$$z(0,t) = pw(0,t) + \bar{c}U(t), \tag{14}$$

$$z_t(x,t) = -q_1 z_x(x,t) - g_2 w(x,t) - g_1 z(x,t), \tag{15}$$

$$w_t(x,t) = q_2 w_x(x,t) - g_4 w(x,t) - g_3 z(x,t), \tag{16}$$

$$w(1,t) = qz(1,t) + c\zeta(t), \tag{17}$$

$$\dot{\zeta}(t) = a_1\zeta(t) - b_1 z(1,t), \tag{18}$$

$\forall (x,t) \in [0,1]\times[0,\infty)$, and the output measurement is

$$Y_{\text{out}}(t) = [\zeta(t-\tau), \dot{\zeta}(t-\tau)]^T, \quad t \in [\tau,\infty) \tag{19}$$

according to the obtained signals shown in (5)–(7). The scalar $\zeta(t)$ is an ODE state. The scalars $z(x,t)$, $w(x,t)$ are states of the 2×2 coupled hyperbolic PDEs. The positive parameter τ is an arbitrary constant denoting the time delay in the measurement. The control input $U(t)$ in (14) is to be designed. The parameters $g_1, g_2, g_3, g_4, c \in \mathbb{R}$ are arbitrary. The positive constants q_1 and q_2 are transport speeds. The constants a_1 and $b_1 \neq 0$ are arbitrary. The parameters $q, p \in \mathbb{R}$ ($q \neq 0$) satisfy Assumption 1.

Assumption 1. The plant parameters p, q satisfy $|pq| < e^{\frac{g_4}{q_2}+\frac{g_1}{q_1}}$.

One can readily check that Assumption 1, which will be used in Section 5, is satisfied in the DCV model with the parameters (12), (13), whose values are given in Table 1.

2.4. Rewrite delay as a transport PDE

By defining $v(x,t) = \zeta(t-\tau(x-1))$, we obtain from (19) a transport PDE

$$v(1,t) = \zeta(t), \tag{20}$$

$$v_t(x,t) = -\frac{1}{\tau}v_x(x,t), \quad x \in [1,2] \tag{21}$$

$$Y_{\text{out}}(t) = [v(2,t), v_t(2,t)]^T \tag{22}$$

for all $(x,t) \in [1,2]\times[0,\infty)$, to describe the time delay in the measurement (19). Replacing (19) by (20)–(22), we obtain a hyperbolic PDE–ODE system connecting with another transport PDE, i.e., the coupled hyperbolic PDEs–ODE–transport PDE system (14)–(18), (20)–(22). The time delay is "removed" at a cost of adding a transport PDE into the plant (14)–(18). The continuous-in-time boundary control design for a PDE–ODE–PDE configuration was also studied in Aarsnes, Vazquez, Di Meglio, and Krstic (2019).

Now, the task is equivalent to exponentially stabilizing the overall system (14)–(18), (20)–(22), i.e., (z,w,v)-PDEs and ζ-ODE by employing an event-triggered output-feedback control input $U(t)$ applying at the left boundary of z-PDE, only using the right boundary state of v-PDE.

3. Observer design

In order to build the observer-based event-triggered output-feedback controller of the plant (14)–(19), in this section, we design a state-observer to track the overall system (14)–(19) using only the delayed measurement $y_{\text{out}}(t)$. Through the reformulation in Section 2, the estimation task is equivalent to designing a state-observer to recover the overall system (14)–(18), (20)–(22) only using the measurements at the right boundary $x=2$ of the v-PDE. The observer is built as a copy of the plant (14)–(18), (20)–(22) plus some output error injection terms, as follows:

$$\hat{z}(0,t) = p\hat{w}(0,t) + \bar{c}U(t), \tag{23}$$

$$\hat{z}_t(x,t) = -q_1\hat{z}_x(x,t) - g_2\hat{w}(x,t) - g_1\hat{z}(x,t), + H_2(x)(Y_{\text{out}}(t) - \hat{Y}_{\text{out}}(t)), \quad x \in [0,1] \tag{24}$$

$$\hat{w}_t(x,t) = q_2\hat{w}_x(x,t) - g_4\hat{w}(x,t) - g_3\hat{z}(x,t) + H_3(x)(Y_{\text{out}}(t) - \hat{Y}_{\text{out}}(t)), \quad x \in [0,1] \tag{25}$$

$$\hat{w}(1,t) = q\hat{z}(1,t) + c\hat{\zeta}(t) + H_4(Y_{\text{out}}(t) - \hat{Y}_{\text{out}}(t)), \tag{26}$$

$$\dot{\hat{\zeta}}(t) = a_1\hat{\zeta}(t) - b_1\hat{z}(1,t) + H_1(Y_{\text{out}}(t) - \hat{Y}_{\text{out}}(t)), \tag{27}$$

$$\hat{v}(1,t) = \hat{\zeta}(t), \tag{28}$$

$$\hat{v}_t(x,t) = -\frac{1}{\tau}\hat{v}_x(x,t) + H_5(x)(Y_{\text{out}}(t) - \hat{Y}_{\text{out}}(t)), \quad x \in [1,2] \tag{29}$$

where

$$\hat{Y}_{\text{out}}(t) = [\hat{v}(2,t), \hat{v}_t(2,t)]^T, \tag{30}$$

and the row vectors $H_1 = [H_{1a}, H_{1b}] \in \mathbb{R}^2$, $H_2(x) = [H_{2a}(x), H_{2b}(x)] \in \mathbb{R}^2$, $H_3(x) = [H_{3a}(x), H_{3b}(x)] \in \mathbb{R}^2$, $H_4 = [H_{4a}, H_{4b}] \in \mathbb{R}^2$, $H_5(x) = [H_{5a}(x), H_{5b}(x)] \in \mathbb{R}^2$ are observer gains to be determined. Defining the observer error states as

$$(\tilde{z}(x,t), \tilde{w}(x,t), \tilde{\zeta}(t), \tilde{v}(x,t)) = (z(x,t), w(x,t), \zeta(t), v(x,t)) - (\hat{z}(x,t), \hat{w}(x,t), \hat{\zeta}(t), \hat{v}(x,t)), \tag{31}$$

according to (14)–(18), (20)–(22) and (23)–(29), the observer error system is obtained as

$$\tilde{z}(0,t) = p\tilde{w}(0,t), \tag{32}$$

$$\tilde{z}_t(x,t) = -q_1\tilde{z}_x(x,t) - g_2\tilde{w}(x,t) - g_1\tilde{z}(x,t) - H_2(x)[\tilde{v}(2,t), \tilde{v}_t(2,t)]^T, \quad x \in [0,1] \tag{33}$$

$$\tilde{w}_t(x,t) = q_2\tilde{w}_x(x,t) - g_4\tilde{w}(x,t) - g_3\tilde{z}(x,t) - H_3(x)[\tilde{v}(2,t), \tilde{v}_t(2,t)]^T, \quad x \in [0,1] \tag{34}$$

$$\tilde{w}(1,t) = q\tilde{z}(1,t) + c\tilde{\zeta}(t) - H_4[\tilde{v}(2,t), \tilde{v}_t(2,t)]^T, \tag{35}$$

$$\dot{\tilde{\zeta}}(t) = a_1\tilde{\zeta}(t) - b_1\tilde{z}(1,t) - H_1[\tilde{v}(2,t), \tilde{v}_t(2,t)]^T, \tag{36}$$

$$\tilde{v}(1,t) = \tilde{\zeta}(t), \tag{37}$$

$$\tilde{v}_t(x,t) = -\frac{1}{\tau}\tilde{v}_x(x,t) - H_5[\tilde{v}(2,t), \tilde{v}_t(2,t)]^T, \ x \in [1,2]. \tag{38}$$

The determination of the observer gains H_1, $H_2(x)$, $H_3(x)$, H_4, $H_5(x)$ in (23)–(29) will be completed through two transformations presented next, which convert the observer error system (32)–(38) to a target observer error system whose exponential stability is straightforward to obtain.

3.1. First transformation

Introduce the transformation

$$\tilde{v}(x,t) = \tilde{\eta}(x,t) + \varphi(x)\tilde{\zeta}(t), \tag{39}$$

where

$$\varphi(x) = e^{-\tau a_1(x-1)}, \quad x \in [1,2], \tag{40}$$

with the purpose of converting (36)–(38) to

$$\dot{\tilde{\zeta}}(t) = -\bar{a}_1\tilde{\zeta}(t) - b_1\tilde{z}(1,t) - e^{\tau a_1}L_1\tilde{\eta}(2,t), \tag{41}$$

$$\tilde{\eta}(1,t) = 0, \tag{42}$$

$$\tilde{\eta}_t(x,t) = -\frac{1}{\tau}\tilde{\eta}_x(x,t), \quad x \in [1,2] \tag{43}$$

where

$$\bar{a}_1 = L_1 - a_1 > 0, \tag{44}$$

by choosing the design parameter L_1. Matching (36) and (41) via (39), by virtue of (44), we obtain that H_1 should satisfy

$$H_1 = [e^{\tau a_1}L_1, 0]. \tag{45}$$

Taking the time and spatial derivatives of (39) and submitting the result into (38), applying (36), (43), and (45), we obtain

$$\begin{aligned}
&\tilde{v}_t(x,t) + \frac{1}{\tau}\tilde{v}_x(x,t) + H_5(x)[\tilde{v}(2,t), \tilde{v}_t(2,t)]^T \\
&= \tilde{\eta}_t(x,t) + \varphi(x)a_1\tilde{\zeta}(t) - \varphi(x)b_1\tilde{z}(1,t) - \varphi(x)e^{\tau a_1}L_1\tilde{v}(2,t) \\
&\quad + \frac{1}{\tau}\tilde{\eta}_x(x,t) + \frac{1}{\tau}\varphi'(x)\tilde{\zeta}(t) + H_5(x)[\tilde{v}(2,t), \tilde{v}_t(2,t)]^T \\
&= -\varphi(x)b_1\tilde{z}(1,t) - \varphi(x)e^{\tau a_1}L_1\tilde{v}(2,t) + H_5(x)[\tilde{v}(2,t), \tilde{v}_t(2,t)]^T \\
&\quad + \left[\varphi(x)a_1 + \frac{1}{\tau}\varphi'(x)\right]\tilde{\zeta}(t) = 0,
\end{aligned} \tag{46}$$

where $\varphi'(x) + \tau a_1\varphi(x) = 0$ obtained from (40) has been used. The row vector $H_5(x)$ are determined to ensure

$$\begin{aligned}
&-\varphi(x)b_1\tilde{z}(1,t) - \varphi(x)e^{\tau a_1}L_1\tilde{v}(2,t) \\
&+ H_5(x)[\tilde{v}(2,t), \tilde{v}_t(2,t)]^T = 0.
\end{aligned} \tag{47}$$

We solve the observer gains by using the Laplace transformations, considering the convenience from the algebraic relationships between the output error injections and other observer error states in the frequency domain.

First, we derive the algebraic relationships between $\tilde{z}(1,s)$ and $\tilde{v}(2,s)$. Taking the Laplace transform of (41), we get

$$(s + \bar{a}_1)\tilde{\zeta}(s) = -b_1\tilde{z}(1,s) - e^{\tau a_1}L_1e^{-\tau s}\tilde{\eta}(1,s). \tag{48}$$

For brevity, we consider all initial conditions to be zero when we take the Laplace transform. (Arbitrary initial conditions could be incorporated into the stability statement through an expanded analysis which is routine but heavy on additional notation.) Recalling (42), and $\bar{a}_1 > 0$ which ensures the fact that $(s + \bar{a}_1)$ does not have any zeros in the closed right-half plane, we obtain from (48) that

$$\tilde{\zeta}(s) = -(s + \bar{a}_1)^{-1}b_1\tilde{z}(1,s). \tag{49}$$

According to (39), (42), (43), applying (40), (49), we have that

$$\tilde{v}(2,s) = e^{-\tau s}\tilde{\eta}(1,s) + \varphi(2)\tilde{\zeta}(s) = -r(s)\tilde{z}(1,s), \tag{50}$$

where

$$r(s) = e^{-\tau a_1}(s + \bar{a}_1)^{-1}b_1. \tag{51}$$

The function $r(s)$ is an asymptotically stable and strictly proper transfer function, according to $\bar{a}_1 > 0$ and Definition 1 taken from Curtain and Morris (2009).

Definition 1. The function G is said to be proper if for, sufficiently large ρ, $\sup_{\mathrm{Re}(s)\geq 0 \bigcap |s|>\rho} |G(s)| < \infty$. If the limit of $G(s)$ at infinity exists and is 0, we say that G is strictly proper.

After obtaining the algebraic relationship (50), we determine H_5 to make (47) hold. Taking the Laplace transform of (47), inserting (40), and (50), we obtain

$$\begin{aligned}
&-\varphi(x)b_1\tilde{z}(1,s) - \varphi(x)e^{\tau a_1}L_1\tilde{v}(2,s) + H_5(x)[\tilde{v}(2,s), s\tilde{v}(2,s)]^T \\
&= -\varphi(x)b_1\tilde{z}(1,s) + \varphi(x)e^{\tau a_1}L_1r(s)\tilde{z}(1,s) \\
&\quad -H_{5a}(s;x)r(s)\tilde{z}(1,s) - H_{5b}(s;x)(e^{-\tau a_1}b_1 - \bar{a}_1r(s))\tilde{z}(1,s) \\
&= -(\varphi(x)b_1 + H_{5b}(s;x)e^{-\tau a_1}b_1)\tilde{z}(1,s) \\
&\quad + (\varphi(x)e^{\tau a_1}L_1 + H_{5b}(s;x)\bar{a}_1 - H_{5a}(s;x))r(s)\tilde{z}(1,s) \\
&= 0,
\end{aligned} \tag{52}$$

where

$$sr(s) = (s + \bar{a}_1 - \bar{a}_1)e^{-\tau a_1}(s + \bar{a}_1)^{-1}b_1 = e^{-\tau a_1}b_1 - \bar{a}_1r(s) \tag{53}$$

by recalling (51), has been used. For (52) to hold, the transfer function $H_5(x)$ is then defined as

$$H_5(x) = [e^{-\tau a_1(x-2)}L_1 - e^{-\tau a_1(x-2)}\bar{a}_1, -e^{-\tau a_1(x-2)}]. \tag{54}$$

In the above derivation, we have completed the conversion between (36)–(38) and (41)–(43) through (39), under the designed $H_1, H_5(x)$. In what follows, H_4 is determined to make $\tilde{w}(1,t)$ in the boundary condition (35) be zero, i.e., to render

$$\tilde{w}(1,t) = q\tilde{z}(1,t) + c\tilde{\zeta}(t) - H_4[\tilde{v}(2,t), \tilde{v}_t(2,t)]^T = 0. \tag{55}$$

Taking the Laplace transform of (55), inserting (49), and (50), we obtain

$$\begin{aligned}
\tilde{w}(1,s) &= q\tilde{z}(1,s) + c\tilde{\zeta}(s) - H_{4a}(x)\tilde{v}(2,s) - H_{4b}s\tilde{v}(2,s) \\
&= q\tilde{z}(1,s) - c(s + \bar{a}_1)^{-1}b_1\tilde{z}(1,s) + H_{4a}r(s)\tilde{z}(1,s) \\
&\quad + H_{4b}sr(s)\tilde{z}(1,s) \\
&= q\tilde{z}(1,s) - ce^{\tau a_1}r(s)\tilde{z}(1,s) \\
&\quad + H_{4a}r(s)\tilde{z}(1,s) + H_{4b}(e^{-\tau a_1}b_1 - \bar{a}_1r(s))\tilde{z}(1,s) \\
&= (q + H_{4b}e^{-\tau a_1}b_1)\tilde{z}(1,s) + (H_{4a} - H_{4b}\bar{a}_1 - ce^{\tau a_1}) \\
&\quad \times r(s)\tilde{z}(1,s) \\
&= 0,
\end{aligned} \tag{56}$$

where (51), (53) have been used. For (56) to hold, the row vector H_4 is chosen as

$$H_4 = \left[-\frac{q\bar{a}_1}{e^{-\tau a_1}b_1} + ce^{\tau a_1}, -\frac{q}{e^{-\tau a_1}b_1}\right]. \tag{57}$$

Through applying the first transformation (39), with H_4, $H_5(x)$, and H_1, then (32)–(38) is converted to the intermediate system as

$$\tilde{z}(0,t) = p\tilde{w}(0,t), \tag{58}$$

$$\tilde{z}_t(x,t) = -q_1\tilde{z}_x(x,t) - g_2\tilde{w}(x,t) - g_1\tilde{z}(x,t) - H_2(x)[\tilde{v}(2,t), \tilde{v}_t(2,t)]^T, \tag{59}$$

$$\tilde{w}_t(x,t) = q_2\tilde{w}_x(x,t) - g_4\tilde{w}(x,t) - g_3\tilde{z}(x,t) - H_3(x)[\tilde{v}(2,t), \tilde{v}_t(2,t)]^T, \tag{60}$$

$$\tilde{w}(1,t) = 0, \tag{61}$$

$$\dot{\tilde{\zeta}}(t) = -\bar{a}_1\tilde{\zeta}(t) - b_1\tilde{z}(1,t) - e^{\tau a_1}L_1\tilde{\eta}(2,t), \tag{62}$$

$$\tilde{\eta}(1,t) = 0, \tag{63}$$

$$\tilde{\eta}_t(x,t) = -\frac{1}{\tau}\tilde{\eta}_x(x,t). \tag{64}$$

Next, we introduce the second transformation to decouple the couplings in (59), (60).

3.2. Second transformation

We now apply the second transformation (Bin & Di Meglio, 2016)

$$\tilde{w}(x,t) = \tilde{\beta}(x,t) - \int_x^1 \psi(x,y)\tilde{\alpha}(y,t)dy, \tag{65}$$

$$\tilde{z}(x,t) = \tilde{\alpha}(x,t) - \int_x^1 \phi(x,y)\tilde{\alpha}(y,t)dy, \tag{66}$$

with the kernels $\psi(x,y)$, $\phi(x,y)$ satisfying

$$\psi(x,x) = \frac{g_3}{q_1+q_2}, \tag{67}$$

$$\phi(0,y) = p\psi(0,y), \tag{68}$$

$$q_2\psi_x(x,y) - q_1\psi_y(x,y) - g_3\phi(x,y) + (g_1-g_4)\psi(x,y) = 0, \tag{69}$$

$$q_1\phi_x(x,y) + q_1\phi_y(x,y) + g_2\psi(x,y) = 0, \tag{70}$$

whose well-posedness is proved in Vazquez et al. (2011). The purpose of the transformations (65), (66) is to convert the intermediate system (58)–(64) to the target system (the subsystem $\tilde{\eta}(\cdot,t)$, given in (63), (64), is removed for brevity because $\tilde{\eta}(\cdot,t) \equiv 0$, $t \geq \tau$), as follows,

$$\tilde{\alpha}(0,t) = p\tilde{\beta}(0,t), \tag{71}$$

$$\tilde{\alpha}_t(x,t) = -q_1\tilde{\alpha}_x(x,t) + \int_x^1 \bar{M}(x,y)\tilde{\beta}(y,t)dy - g_1\tilde{\alpha}(x,t) - g_2\tilde{\beta}(x,t), \tag{72}$$

$$\tilde{\beta}_t(x,t) = q_2\tilde{\beta}_x(x,t) + \int_x^1 \bar{N}(x,y)\tilde{\beta}(y,t)dy - g_4\tilde{\beta}(x,t), \tag{73}$$

$$\tilde{\beta}(1,t) = 0, \tag{74}$$

$$\dot{\tilde{\zeta}}(t) = -\bar{a}_1\tilde{\zeta}(t) - b_1\tilde{\alpha}(1,t), \tag{75}$$

for $t \geq \tau$, where the integral operator kernels $\bar{M}$ and $\bar{N}$ are defined as

$$\bar{M}(x,y) = \int_x^y \phi(x,\delta)\bar{M}(\delta,y)d\delta - g_2\phi(x,y), \tag{76}$$

$$\bar{N}(x,y) = \int_x^y \psi(x,\delta)\bar{M}(\delta,y)d\delta - g_2\psi(x,y). \tag{77}$$

In what follows, $H_2(x)$, $H_3(x)$ are determined by matching the intermediate system (58)–(62) and the target observer error system (71)–(75) via (65), (66). Inserting (65), (66) into (60) along (72), (73), and applying (67)–(69), (77), we get

$$\begin{aligned}&\tilde{w}_t(x,t) - q_2\tilde{w}_x(x,t) + g_3\tilde{z}(x,t) + g_4\tilde{w}(x,t) \\ &\quad + H_3(x)[\tilde{v}(2,t), \tilde{v}_t(2,t)]^T \\ &= q_1\psi(x,1)\tilde{\alpha}(1,t) + H_3(x)[\tilde{v}(2,t), \tilde{v}_t(2,t)]^T = 0,\end{aligned} \tag{78}$$

where the detailed calculation is omitted here due to space limit. We thus know that the following equation needs to be satisfied

$$q_1\psi(x,1)\tilde{z}(1,t) + H_3(x)[\tilde{v}(2,t), \tilde{v}_t(2,t)]^T = 0, \tag{79}$$

where $\tilde{\alpha}(1,t) = \tilde{z}(1,t)$ according to (66) has been used. Rewriting (79) in the frequency domain and applying (50), (53), we obtain

$$\begin{aligned}&q_1\psi(x,1)\tilde{z}(1,s) + H_3(x)[\tilde{v}(2,s), s\tilde{v}(2,s)]^T \\ &= q_1\psi(x,1)\tilde{z}(1,s) - H_{3a}(x)r(s)\tilde{z}(1,s) \\ &\quad -H_{3b}(x)(e^{-\tau a_1}b_1 - \bar{a}_1 r(s))\tilde{z}(1,s) \\ &= (q_1\psi(x,1) - H_{3b}(x)e^{-\tau a_1}b_1)\tilde{z}(1,s) \\ &\quad + (H_{3b}(x)\bar{a}_1 - H_{3a}(x))r(s)\tilde{z}(1,s) = 0.\end{aligned} \tag{80}$$

The transfer function $H_3(x)$ is chosen as

$$H_3(x) = \left[\frac{\bar{a}_1 q_1\psi(x,1)}{e^{-\tau a_1}b_1}, \frac{q_1\psi(x,1)}{e^{-\tau a_1}b_1}\right]. \tag{81}$$

Inserting (65), (66) into (59) along (72), (73), applying (70), (76), we get

$$\begin{aligned}&\tilde{z}_t(x,t) + q_1\tilde{z}_x(x,t) + g_2\tilde{w}(x,t) + g_1\tilde{z}(x,t) \\ &\quad + H_2(x)[\tilde{v}(2,t), \tilde{v}_t(2,t)]^T \\ &= q_1\phi(x,1)\tilde{\alpha}(1,t) + H_2(x)[\tilde{v}(2,t), \tilde{v}_t(2,t)]^T = 0\end{aligned} \tag{82}$$

where the detailed calculation is omitted here due to space limit. Therefore, $H_2(x)[\tilde{v}(2,t), \tilde{v}_t(2,t)]^T$ should satisfy

$$q_1\phi(x,1)\tilde{z}(1,t) + H_2(x)[\tilde{v}(2,t), \tilde{v}_t(2,t)]^T = 0 \tag{83}$$

where $\tilde{\alpha}(1,t) = \tilde{z}(1,t)$ according to (66) has been used. Taking the Laplace transform of (83), and recalling (50), (53), we obtain

$$\begin{aligned}&q_1\phi(x,1)\tilde{z}(1,s) + H_2(x)[\tilde{v}(2,s), s\tilde{v}(2,s)]^T \\ &= q_1\phi(x,1)\tilde{z}(1,s) - H_{2a}(x)r(s)\tilde{z}(1,s) \\ &\quad -H_{2b}(x)(e^{-\tau a_1}b_1 - \bar{a}_1 r(s))\tilde{z}(1,s) \\ &= (q_1\phi(x,1) - H_{2b}(x)e^{-\tau a_1}b_1)\tilde{z}(1,s) \\ &\quad + (H_{2b}(x)\bar{a}_1 - H_{2a}(x))r(s)\tilde{z}(1,s) = 0.\end{aligned} \tag{84}$$

The transfer function $H_2(x)$ is determined as

$$H_2(x) = \left[\frac{\bar{a}_1 q_1\phi(x,1)}{e^{-\tau a_1}b_1}, \frac{q_1\phi(x,1)}{e^{-\tau a_1}b_1}\right]. \tag{85}$$

The boundary condition (71), follows directly from inserting $x = 0$ into (65), (66) and applying (58), (68). The second conversion is thus completed and two PDEs (59), (60) are decoupled now, which can be seen in (72), (73).

After the above two transformations, we have converted the original observer error system (32)–(38) to the target observer error system (71)–(75) (for $t \in [\tau, \infty)$, $\tilde{\eta}(x,t) \equiv 0$ according to (63), (64) is removed for brevity). The well-posedness and exponential convergence of the observer error system are shown in the next subsection, which guarantees the output error injections in the observer (23)–(29) are well-defined and exponentially convergent to zero.

3.3. Stability analysis of the observer error system

Lemma 1. *For all initial conditions* $(\tilde{z}[0], \tilde{w}[0])^T \in C^0([0,1]; \mathbb{R}^2)$, $\tilde{v}[0] \in C^1([1,2]; \mathbb{R})$, *and* $\tilde{\zeta}(0) \in \mathbb{R}$, *there exists a unique solution* $(\tilde{z}[t], \tilde{w}[t])^T \in C^0(\mathbb{R}^+; \mathbb{R}^2)$, $\tilde{v}[t] \in C^1(\mathbb{R}^+; \mathbb{R})$, $\tilde{\zeta}(t) \in C^1(\mathbb{R}^+; \mathbb{R})$ *to the system* (32)–(38).

Proof. Because of $\tilde{v}[0] \in C^1([1,2];\mathbb{R})$, we have that $\tilde{\eta}[0] \in C^1([1,2];\mathbb{R})$ recalling (39), (40). We then obtain that $\tilde{\eta}[t] \in C^1([1,2];\mathbb{R})$ according to (42), (43). The target observer error system on $t \in [0,\infty)$ is (71)–(75) plus $\tilde{\eta}$ dynamics in (42), (43), where $\tilde{\eta}(2,t) \in C^1$ goes into (75). Recalling the initial condition in this lemma and the inverse backstepping transformation (65), (66), we have that $(\tilde{\alpha}[0], \tilde{\beta}[0])^T \in C^0([0,1];\mathbb{R}^2)$, $\tilde{\eta}[0] \in C^1([1,2];\mathbb{R})$. Therefore, according to Theorem 2.6 in Karafyllis and Krstic (2019), we obtain that there exists a unique solution $(\tilde{\alpha}[t], \tilde{\beta}[t])^T \in C^0(\mathbb{R}^+;\mathbb{R}^2)$, $\tilde{\zeta}(t) \in C^1(\mathbb{R}^+;\mathbb{R})$ to the system: (71)–(75) with an external input $\tilde{\eta}(2,t) \in C^1(\mathbb{R}^+;\mathbb{R})$ entering (75). Recalling the backstepping transformation (65), (66), and (39), the proof of this lemma is complete. □

Theorem 1. *For all initial data* $((\tilde{z}[0], \tilde{w}[0])^T, \tilde{v}[0], \tilde{\zeta}(0)) \in C^0([0,1];\mathbb{R}^2) \times C^1([1,2];\mathbb{R}) \times \mathbb{R}$, *and* $m(0) \in \mathbb{R}^-$, *the exponential convergence of the observer error system* (32)–(38) *holds in the sense of the norm* $\|\tilde{z}(\cdot,t)\|_\infty + \|\tilde{w}(\cdot,t)\|_\infty + \|\tilde{v}(\cdot,t)\|_\infty + \|\tilde{v}_t(\cdot,t)\|_\infty + |\tilde{\zeta}(t)| + |\dot{\tilde{\zeta}}(t)|$, *where the decay rate is adjustable by* L_1 *through* (44).

Proof. The stability of the original observer error system is obtained by analyzing the stability of the target observer error system (71)–(75) with (63), (64), and using the transformations (39), and (65), (66).

With the method of characteristics, it is easy to show that $\tilde{\beta}[t] \equiv 0$ after $t = \tau + \frac{1}{q_2}$ considering (73), (74). According to (71), (72), we have that $\tilde{\alpha}[t] \equiv 0$ after $t_0 = \tau + \frac{1}{q_1} + \frac{1}{q_2}$. Because of $\bar{a}_1 > 0$, we then have that $\tilde{\zeta}(t)$ is exponentially convergent to zero after t_0. Recalling $\tilde{\eta}[t] \equiv 0$ after $t = \tau$, we obtain that $\tilde{\eta}_t(x,t) \equiv 0$ for $t \geq \tau$. According to $\tilde{\alpha}(1,t) \equiv 0$ and the fact that $\tilde{\zeta}(t)$ is exponentially convergent to zero, after t_0, we obtain that $\tilde{\zeta}(t)$ is exponentially convergent to zero after t_0 via (75). Therefore, we have that $\bar{\Omega}(t) = \|\tilde{\alpha}(\cdot,t)\|_\infty + \|\tilde{\beta}(\cdot,t)\|_\infty + \|\tilde{\eta}(\cdot,t)\|_\infty + \|\tilde{\eta}_t(\cdot,t)\|_\infty + |\tilde{\zeta}(t)| + |\dot{\tilde{\zeta}}(t)|$ is bounded by an exponential decay with the decay rate λ_e for $t \geq t_0$. The decay rate λ_e depends on the decay rate of the ODE $\tilde{\zeta}(t)$. In other words, the decay rate λ_e depends on the choice of L_1 according to (44). It should be noted that the transient in the finite time $[0,t_0)$ can be bounded by an arbitrarily fast decay rate considering a trade off between the decay rate and the overshoot coefficient, i.e., the higher the decay rate, the higher the overshoot coefficient. Therefore, we conclude the exponential stability in the sense that $\bar{\Omega}(t)$ is bounded by an exponential decay rate λ_e with some overshoot coefficients for $t \geq 0$. Applying the transformations (39), and (65), (66), we respectively have that $\|\tilde{v}(\cdot,t)\|_\infty \leq \Upsilon_{1a}(\|\tilde{\eta}(\cdot,t)\|_\infty + |\tilde{\zeta}(t)|)$, $\|\tilde{v}_t(\cdot,t)\|_\infty \leq \Upsilon_{1b}(\|\tilde{\eta}_t(\cdot,t)\|_\infty + |\tilde{\zeta}(t)|)$, $\|\tilde{z}(\cdot,t)\|_\infty + \|\tilde{w}(\cdot,t)\|_\infty \leq \Upsilon_{1c}(\|\tilde{\alpha}(\cdot,t)\|_\infty + \|\tilde{\beta}(\cdot,t)\|_\infty)$, for some positive Υ_{1a}, Υ_{1b}, Υ_{1c}. The proof is complete. □

4. Output-feedback control design

In the last section, we have obtained the observer which compensates the time-delay in the output measurements of the distal ODE, to track the states of the overall system (14)–(19). In this section, we design an output-feedback control law $U(t)$ based on the observer (23)–(29) with output estimation error injection terms assumed absent for reducing notation burden, in accordance to the result on their convergence to zero in Theorem 1. The separation principle is then verified in the resulting output-feedback closed-loop system.

With the purpose of removing the coupling terms in (24), (25), and making the system parameter in the distal ODE (27) to be negative, a PDE backstepping transformation in the following form (Meglio, Bribiesca, Hu, & Krstic, 2018)

$$\alpha(x,t) = \hat{z}(x,t) - \int_x^1 K_3(x,y)\hat{z}(y,t)dy - \int_x^1 J_3(x,y)\hat{w}(y,t)dy - \gamma(x)\hat{\zeta}(t), \tag{86}$$

$$\beta(x,t) = \hat{w}(x,t) - \int_x^1 K_2(x,y)\hat{z}(y,t)dy - \int_x^1 J_2(x,y)\hat{w}(y,t)dy - \lambda(x)\hat{\zeta}(t) \tag{87}$$

is introduced, where the kernels $K_3(x,y)$, $J_3(x,y)$, $\gamma(x)$, $K_2(x,y)$, $J_2(x,y)$, $\lambda(x)$ satisfy

$$K_3(x,1) = \frac{q_2 q}{q_1} J_3(x,1) - \frac{b_1}{q_1}\gamma(x), \tag{88}$$

$$J_3(x,x) = \frac{g_2}{q_2+q_1}, \tag{89}$$

$$-q_1 J_{3x}(x,y) + q_2 J_{3y}(x,y) + g_2 K_3(x,y) - (g_1 - g_4) J_3(x,y) = 0, \tag{90}$$

$$-q_1 K_{3x}(x,y) - q_1 K_{3y}(x,y) + g_3 J_3(x,y) = 0, \tag{91}$$

$$\gamma(1) = F_1, \tag{92}$$

$$-q_1\gamma'(x) - \gamma(x)(a_1 + g_1) - q_2 J_3(x,1)c = 0, \tag{93}$$

$$J_2(x,1) = \frac{q_1}{q_2 q} K_2(x,1) + \frac{b_1}{q_2 q}\lambda(x), \tag{94}$$

$$K_2(x,x) = \frac{-g_3}{q_1+q_2}, \tag{95}$$

$$q_2 J_{2x}(x,y) + q_2 J_{2y}(x,y) + g_2 K_2(x,y) = 0, \tag{96}$$

$$q_2 K_{2x}(x,y) - q_1 K_{2y}(x,y) + g_3 J_2(x,y) + (g_1 - g_4) K_2(x,y) = 0, \tag{97}$$

$$q_2\lambda'(x) - \lambda(x)(a_1 + g_4) - q_2 J_2(x,1)c = 0, \tag{98}$$

$$\lambda(1) = q\gamma(1) + c \tag{99}$$

to convert (23)–(29) (without output estimation error injections) into the target system:

$$\alpha(0,t) = p\beta(0,t), \tag{100}$$

$$\alpha_t(x,t) = -q_1\alpha_x(x,t) - g_1\alpha(x,t), \tag{101}$$

$$\beta_t(x,t) = q_2\beta_x(x,t) - g_4\beta(x,t), \tag{102}$$

$$\beta(1,t) = q\alpha(1,t), \tag{103}$$

$$\dot{\hat{\zeta}}(t) = -a_{\mathrm{m}}\hat{\zeta}(t) - b_1\alpha(1,t), \tag{104}$$

$$\hat{v}(1,t) = \hat{\zeta}(t), \tag{105}$$

$$\hat{v}_t(x,t) = -\frac{1}{\tau}\hat{v}_x(x,t), \tag{106}$$

where

$$a_{\mathrm{m}} = b_1 F_1 - a_1 > 0 \tag{107}$$

is made by choosing the design parameter F_1, with choosing the control input as

$$U(t) = \frac{1}{\bar{c}}\int_0^1 \bar{K}_1(x)\hat{z}(x,t)dx + \frac{1}{\bar{c}}\int_0^1 \bar{K}_2(x)\hat{w}(x,t)dx + \frac{1}{\bar{c}}\bar{K}_3\hat{\zeta}(t) \tag{108}$$

where $\bar{K}_1(x) = K_3(0,x) - pK_2(0,x)$, $\bar{K}_2(x) = J_3(0,x) - pJ_2(0,x)$, $\bar{K}_3 = \gamma(0) - p\lambda(0)$.

The conditions of the kernels (88)–(99) are obtained by matching (101)–(104) and (24)–(27). The equation sets (88)–(93) and (94)–(99) have the analogous structure with (19)–(24) in Wang, Krstic et al. (2018). Following the proof of Lemma 1 in Wang, Krstic et al. (2018), we obtain the well-posedness of (88)–(99). Following Section 2.4 in Wang, Krstic et al. (2018), we have that the inverse transformation of (86), (87) exists, and the well-posedness of the kernels in the inverse transformation can be obtained from the well-posedness of (88)–(99).

5. Event-triggering mechanism

In this section we introduce an event-triggered control scheme for stabilization of the overall PDE–ODE–PDE system (14)–(18), (20)–(22). This scheme relies on both the delay-compensated observer-based output-feedback continuous-in-time controller designed in the last section, and a dynamic event-triggering mechanism (ETM) which is realized using the states from the delay-compensated observer. The event-triggered control signal $U_d(t)$ is the value of the continuous-in-time control signal $U(t)$ at the time instants t_k but applied until time t_{k+1}, i.e.,

$$U_d(t) = U(t_k) = \frac{1}{\bar{c}}\int_0^1 \bar{K}_1(x)\hat{z}(x,t_k)dx + \frac{1}{\bar{c}}\int_0^1 \bar{K}_2(x)\hat{w}(x,t_k)dx + \frac{1}{\bar{c}}\bar{K}_3\hat{\zeta}(t_k), \quad t\in[t_k,t_{k+1}). \tag{109}$$

A deviation $d(t)$ between the continuous-in-time control signal and the event-based one is given as

$$d(t) = U(t) - U_d(t). \tag{110}$$

Inserting (109), the left boundary of the target system (100)–(106) becomes

$$\alpha(0,t) = p\beta(0,t) - \bar{c}d(t). \tag{111}$$

Taking the Laplace transform of (101)–(106), according to Section 3.2 in Meglio et al. (2020), we obtain the following algebraic relationship between $\alpha(0,s)$ and $\beta(0,s)$ as

$$\beta(0,s) = qe^{-\frac{(g_4+s)}{q_2}-\frac{(g_1+s)}{q_1}}\alpha(0,s), \tag{112}$$

Inserting (112) into (111) in the frequency domain, we have that

$$\alpha(0,s) = -\frac{\bar{c}}{(1-h(s))}d(s), \tag{113}$$

where

$$h(s) = pqe^{-\left(\frac{g_4}{q_2}+\frac{g_1}{q_1}\right)}e^{-\left(\frac{1}{q_2}+\frac{1}{q_1}\right)s}. \tag{114}$$

From (113), (114), Assumption 1 guarantees

$$|\alpha(0,t)| \le |h(0)| \sup_{0\le\xi\le t}|\alpha(0,\xi)| + |\bar{c}| \sup_{0\le\xi\le t}|d(\xi)|,$$

where the constant $|h(0)|$ is strictly smaller than 1. By the small gain theorem, we obtain

$$\alpha(0,t)^2 \le \lambda_d \sup_{0\le\xi\le t} d(\xi)^2 \tag{115}$$

where

$$\lambda_d = \frac{\bar{c}^2}{(1-|h(0)|)^2}.$$

Please note that we obtain (115), which will be used in the Lyapunov analysis, based on (101)–(106) (state-feedback loop), i.e., assuming the observer error injections absent, with the purpose of avoiding heavy additional notation. Incorporating these observer error injections will not change the stability result obtained in the Lyapunov analysis, which will be shown latter, by virtue of exponential convergence of the observer errors in Theorem 1.

Similar to Espitia et al. (2018), the ETM to determine the triggering times is designed to be governed by the following dynamic triggering condition:

$$t_{k+1} = \inf\{t\in R^+ | t > t_k | d(t)^2 \ge \theta V(t) - \mu m(t)\}. \tag{116}$$

The internal dynamic variable $m(t)$ satisfies the ordinary differential equation

$$\dot{m}(t) = -\eta m(t) - \kappa_1\alpha(1,t)^2 - \kappa_2\alpha(0,t)^2 - \kappa_3\hat{v}(2,t)^2 - \kappa_4\left|\tilde{Y}(t)\right|^2 \tag{117}$$

where

$$\tilde{Y}(t) = Y_{\text{out}}(t) - \hat{Y}_{\text{out}}(t),$$

and where the initial condition of m is $m(0) < 0$, which guarantees that

$$m(t) < 0 \tag{118}$$

for $t \in [0,\infty)$. Inequality (118) follows from the ODE in (117), the nonpositivity of the non-homogeneous terms on its right-hand side, the strict negativity of $m(0)$, the variation-of-constants formula, and the comparison principle. Introducing the internal dynamic variable $m(t)$ defined by (117) is used in proving the existence of a minimal dwell time, which will be seen clearly in the proof of Lemma 3. The Lyapunov function $V(t)$ in (116) is defined as

$$V(t) = \frac{1}{2}\hat{\zeta}(t)^2 + \frac{1}{2}\int_0^1 e^{\delta_1 x}\beta(x,t)^2dx + \frac{1}{2}r_b\int_0^1 e^{-\delta_2 x}\alpha(x,t)^2dx + \frac{1}{2}r_c\int_1^2 e^{-x}\hat{v}(x,t)^2dx. \tag{119}$$

The event-triggering condition, including (116), (117), (119), only uses the output measurement and the observer states, recalling the transformations (86), (87). The positive design parameters θ, μ, η, κ_1, κ_2, κ_3, κ_4, δ_1, δ_2, r_c, r_b satisfy

$$\kappa_1 > 2\lambda_1, \tag{120}$$

$$\kappa_2 > 2\lambda_1, \tag{121}$$

$$\kappa_4 > 2\lambda_1, \tag{122}$$

$$\delta_1 > \frac{2|g_4|}{q_2}, \tag{123}$$

$$\delta_2 > \frac{2|g_1|}{q_1}, \tag{124}$$

$$r_c < a_{\text{m}}e\tau, \tag{125}$$

$$r_b > \frac{1}{q_1}q^2q_2e^{\delta_1+\delta_2} + \frac{b_1^2}{q_1a_{\text{m}}}e^{\delta_2} + \frac{2}{q_1}\kappa_1e^{\delta_2}, \tag{126}$$

$$\kappa_3 < \frac{1}{2\tau}r_ce^{-2}, \tag{127}$$

$$\mu < \frac{\sigma_a}{\frac{1}{2}q_1r_b\lambda_d + \kappa_2\lambda_d}, \tag{128}$$

$$\theta < \min\left\{\frac{\sigma_a}{\frac{1}{2}q_1r_b\lambda_d + \kappa_2\lambda_d}, \frac{\mu\tau}{r_c}\kappa_3e^2, \frac{\mu}{2\lambda_{\alpha1}}\kappa_1, \frac{\mu}{2\lambda_{\alpha0}}\kappa_2, \frac{\mu}{2}\kappa_4\right\}, \tag{129}$$

where η is free and associated with the dwell-time, which can be seen later, and λ_1 is a positive constant, which will be given in Lemma 2, only depending on the plant parameters and the

design parameters L_1, F_1 in the continuous-in-time control law, and where

$$\sigma_a = \min\left\{\lambda_a, \eta, \frac{2\kappa_4}{R_e}\right\} > 0, \tag{130}$$

$$\lambda_a = \frac{1}{\bar{\xi}_2}\min\left\{\frac{1}{2}\left(a_{\rm m} - \frac{1}{\tau}r_c e^{-1}\right), \frac{1}{2}\delta_1 q_2 - |g_4|, \frac{1}{2}\delta_2 q_1 r_b e^{-\delta_2} - r_b|g_1|e^{-\delta_2}, \frac{e^{-2}}{2\tau}r_c\right\}, \tag{131}$$

$$R_e > \frac{2\kappa_4}{\lambda_e}, \tag{132}$$

$$\lambda_{\alpha 1} = \frac{1}{2}|b_1| + \frac{1}{2}q_1 r_b e^{-\delta_2}, \tag{133}$$

$$\lambda_{\alpha 0} = \frac{1}{q^2}q_2 \max\{1, \bar{c}^2\}, \tag{134}$$

where λ_e is a positive constant depending on the design parameters L_1, as shown in proof of Theorem 1.

The conditions of all the parameters L_1, F_1, κ_1, κ_2, κ_4, δ_1, δ_2, r_c, r_b, κ_3, μ, θ, are given in (44), (107), (120)–(129), which are cascaded rather than coupled. An order of selecting these parameters is along (44), (107), (120)–(129). As will be seen later, these design parameters are associated with the dwell-time, convergence rate, and overshoot in the event-based closed-loop system. The optimal choices of these parameters are not studied in this paper, but in the future work the trade off between the convergence rate and the lower bound of the minimal dwell time is worth studying.

Proposition 1. *For given $(z(\cdot,t_k), w(\cdot,t_k))^T \in L^2((0,1);\mathbb{R}^2)$, $v(\cdot,t_k) \in L^2((1,2);\mathbb{R})$, $\zeta(t_k) \in \mathbb{R}$ and $(\hat{z}(\cdot,t_k), \hat{w}(\cdot,t_k))^T \in L^2((0,1);\mathbb{R}^2)$, $\hat{v}(\cdot,t_k) \in L^2((1,2);\mathbb{R})$, $\hat{\zeta}(t_k) \in \mathbb{R}$, $m(t_k) \in \mathbb{R}^-$, there exist a unique (weak) solution $((z,w)^T, v, \zeta) \in C^0([t_k,t_{k+1}];L^2(0,1);\mathbb{R}^2) \times C^0([t_k,t_{k+1}];L^2(1,2)) \times C^0([t_k,t_{k+1}];\mathbb{R})$, $((\hat{z},\hat{w})^T, \hat{v}, \hat{\zeta}) \in C^0([t_k,t_{k+1}];L^2(0,1);\mathbb{R}^2) \times C^0([t_k,t_{k+1}];L^2(1,2)) \times C^0([t_k,t_{k+1}];\mathbb{R})$, $m \in C^0([t_k,t_{k+1}];\mathbb{R}^-)$ to the system (14)–(19), (23)–(29), (117) with the piecewise-constant control input $U_d(t)$ in (109).*

Proof. For given $(z(\cdot,t_k), w(\cdot,t_k))^T \in L^2((0,1);\mathbb{R}^2)$, $v(\cdot,t_k) \in L^2((1,2);\mathbb{R})$, $\zeta(t_k) \in \mathbb{R}$, following the proof in Proposition 1 of Wang and Krstic (2021c), we have that there exists a unique (weak) solution $((z,w)^T, v, \zeta) \in C^0([t_k,t_{k+1}];L^2(0,1);\mathbb{R}^2) \times C^0([t_k,t_{k+1}];L^2(1,2)) \times C^0([t_k,t_{k+1}];\mathbb{R})$ to the system (14)–(19) under the piecewise-constant control input $U_d(t)$. Recalling Lemma 1, (31), and $m(t_k) \in \mathbb{R}^-$, it follows that there exists a unique (weak) solution $((\hat{z},\hat{w})^T, \hat{v}, \hat{\zeta}) \in C^0([t_k,t_{k+1}];L^2(0,1);\mathbb{R}^2) \times C^0([t_k,t_{k+1}];L^2(1,2)) \times C^0([t_k,t_{k+1}];\mathbb{R})$ and $m \in C^0([t_k,t_{k+1}];\mathbb{R}^-)$ to the system (23)–(29) and (117) under the piecewise-constant control input $U_d(t)$. Proposition 1 is thus obtained. □

Lemma 2. *For $d(t)$ defined in (110), there exists a positive constant λ_1 such that*

$$\dot{d}(t)^2 \le \lambda_1\left(\Omega(t) + \alpha(1,t)^2 + \alpha(0,t)^2 + d(t)^2 + \left|\tilde{Y}(t)\right|^2\right) \tag{135}$$

for $t \in (t_k, t_{k+1})$, where

$$\Omega(t) = \|\alpha(\cdot,t)\|^2 + \|\beta(\cdot,t)\|^2 + \hat{\zeta}(t)^2, \tag{136}$$

and where λ_1 only depends on parameters of the plant, and the design parameters L_1, F_1 in the continuous-in-time control law.

Proof. Taking the time derivative of (110), we have $\dot{d}(t)^2 = \dot{U}(t)^2$, because of $\dot{U}_d(t) = 0$ for $t \in (t_k, t_{k+1})$. Recalling (23)–(27), (108), we have

$$\begin{aligned}
\dot{d}(t)^2 = \dot{U}(t)^2 = \frac{1}{\bar{c}^2}\Bigg[&\bar{K}_1(0)q_1\hat{z}(0,t) - q_2\bar{K}_2(0)\hat{w}(0,t)\\
&- \left(\bar{K}_1(1)q_1 - q\bar{K}_2(1)q_2 + \bar{K}_3 b_1\right)\hat{z}(1,t) + (\bar{K}_3 a_1 + c\bar{K}_2(1)q_2)\hat{\zeta}(t)\\
&+ \int_0^L\left(\bar{K}_1'(x)q_1 - \bar{K}_1(x)g_1 - \bar{K}_2(x)g_3\right)\hat{z}(x,t)dx\\
&- \int_0^L\left(\bar{K}_2(x)g_4 - \bar{K}_2'(x)q_2 + \bar{K}_1(x)g_2\right)\hat{w}(x,t)dx\\
&+ \Bigg(\int_0^1 \bar{K}_1(x)H_2(x)dx + \int_0^1 \bar{K}_2(x)H_3(x)dx\\
&+ \bar{K}_3 H_1 + \bar{K}_2(1)q_2 H_4\Bigg)\tilde{Y}(t)\Bigg]^2\\
\le \lambda_0\Bigg[&\hat{z}(1,t)^2 + \hat{w}(0,t)^2 + \hat{z}(0,t)^2 + \|\hat{z}(\cdot,t)\|^2 + \|\hat{w}(\cdot,t)\|^2\\
&+ \hat{\zeta}(t)^2 + \left|\tilde{Y}(t)\right|^2\Bigg]
\end{aligned}$$

for some positive λ_0 only depending on parameters of the plant, and the design parameters L_1, F_1 in the continuous-in-time control law. Recalling the inverse transformation and (111), we obtain (135). The proof of Lemma 2 is complete. □

Remark 1. The target system corresponding to the output-feedback loop is obtained by applying the backstepping transformation (86), (87) into the observer (23)–(29), and replacing U in (23) by U_d defined in (109). The resulting system is (111), (101)–(106) with output estimation error injection terms $G_2(x)\tilde{Y}(t)$, $G_3(x)\tilde{Y}(t)$, $H_4\tilde{Y}(t)$, $H_1\tilde{Y}(t)$, $H_5(x)\tilde{Y}(t)$ in (101), (102), (103), (104), (106), respectively, where the bounded functions G_2, G_3 depend on the observer gains obtained in Section 3 and the kernels in the backstepping transformation (86), (87). In the following analysis, we denote this system as $\mathcal{S}$-system, whose full expression is not displayed here due to the space limit.

The following lemma proves the existence of a minimal dwell-time independent of initial conditions.

Lemma 3. *For some $\kappa_1, \kappa_2, \kappa_4, \theta$, there exists a minimal dwell-time, independent of initial conditions, between any two successive triggering times, i.e., $t_{k+1} - t_k \ge T > 0$ for all $k \ge 0$.*

Proof. Let us introduce the function

$$\psi(t) = \frac{d(t)^2 + \frac{\mu}{2}m(t)}{\theta V(t) - \frac{\mu}{2}m(t)} \tag{137}$$

which is proposed in Espitia et al. (2018). We have that $\psi(t_{k+1}) = 1$ because the event is triggered, and $\psi(t_k) < 0$ because of $m(t) < 0$ and $d(t_k) = 0$. The function $\psi(t)$ is continuous on $[t_k, t_{k+1}]$ due to Proposition 1. By the intermediate value theorem, there exists $t^* > t_k$ such that $\psi(t) \in [0,1]$ when $t \in [t^*, t_{k+1}]$. The lower bound of the minimal dwell-time T can be defined as the minimal time it takes for $\psi(t)$ from 0 to 1, i.e., the reciprocal of the absolute value of the maximum $\dot{\psi}(t)$.

For all $t \in [t^*, t_{i+1}]$, taking the time derivative of $V(t)$ (119) along the $\mathcal{S}$-system defined in Remark 1, the following inequality can be obtained

$$\begin{aligned}
\dot{V}(t) \ge &-\mu_0\Omega_1(t) - \lambda_{\alpha 1}\alpha(1,t)^2 - \lambda_{\alpha 0}(\alpha(0,t)^2 + d(t)^2)\\
&- \frac{1}{2\tau}r_c e^{-2}\hat{v}(2,t)^2 - \left|\tilde{Y}(t)\right|^2
\end{aligned} \tag{138}$$

where

$$\Omega_1(t) = \|\alpha(\cdot,t)\|^2 + \|\beta(\cdot,t)\|^2 + \|\hat{v}(\cdot,t)\|^2 + \hat{\zeta}(t)^2, \tag{139}$$

and $\mu_0 = \max\Big\{\frac{1}{2}\delta_1 q_2 e^{\delta_1} + |g_4|e^{\delta_1} + e^{2\delta_1}\max_{x\in[0,1]}\{G_3(x)^2\}, \frac{1}{2}\delta_2 q_1 r_b + |g_1|r_b + r_b{}^2\max_{x\in[0,1]}\{G_2(x)^2\}, \frac{1}{2\tau}r_c e^{-1} + r_c{}^2\max_{x\in[1,2]}\{H_5(x)^2\}, a_{\rm m} + \frac{1}{2}|b_1| + H_1^2\Big\}$, and where the positive constants $\lambda_{\alpha 1}$, $\lambda_{\alpha 0}$ are shown in (133), (134).

Taking the derivative of (137), applying Young's inequality, using (135) in Lemma 2, and inserting (138), we have

$$\begin{aligned}
\dot{\psi} &= \frac{(2d(t)\dot{d}(t) + \frac{\mu}{2}\dot{m}(t))}{\theta V(t) - \frac{\mu}{2}m(t)} - \frac{(\theta\dot{V}(t) - \frac{\mu}{2}\dot{m}(t))}{\theta V(t) - \frac{\mu}{2}m(t)}\psi \\
&\le \frac{1}{\theta V(t) - \frac{\mu}{2}m(t)}\Big[\mu\lambda_1\Omega(t)^2 + \mu\lambda_1\alpha(1,t)^2 \\
&+ \mu\lambda_1\alpha(0,t)^2 + \Big(\frac{1}{\mu} + \mu\lambda_1\Big)d(t)^2 + \mu\lambda_1\left|\tilde{Y}(t)\right|^2 + \frac{\mu}{2}\dot{m}(t)\Big] \\
&- \frac{1}{\theta V(t) - \frac{\mu}{2}m(t)}\Big[\theta\Big(-\mu_0\Omega_1(t) - \lambda_{\alpha 1}\alpha(1,t)^2 \\
&- \lambda_{\alpha 0}(\alpha(0,t)^2 + d(t)^2) - \frac{1}{2\tau}r_c e^{-2}\hat{v}(2,t)^2 - \left|\tilde{Y}(t)\right|^2\Big) - \frac{\mu}{2}\dot{m}(t)\Big]\psi.
\end{aligned}$$

Inserting (117) to replace $\dot{m}(t)$, recalling (119), (136), (139) and the fact that $\xi_1\Omega_1(t) \le V(t) \le \xi_2\Omega_1(t)$ where the positive constants ξ_1, ξ_2 are $\xi_1 = \min\{\frac{1}{2}, \frac{1}{2}r_b e^{-\delta_2}, \frac{1}{2}r_c e^{-2}\}$ and $\xi_2 = \max\{\frac{1}{2}, \frac{1}{2}e^{\delta_1}, \frac{1}{2}r_b, \frac{1}{2}r_c e^{-1}\}$, we have that

$$\begin{aligned}
\dot{\psi} &\le \frac{1}{\theta V(t) - \frac{\mu}{2}m(t)}\Big[\Big(\frac{1}{\mu} + \mu\lambda_1\Big)d(t)^2 + \Big(\mu\lambda_1 - \frac{\mu}{2}\kappa_1\Big)\alpha(1,t)^2 \\
&+ \Big(\mu\lambda_1 - \frac{\mu}{2}\kappa_2\Big)\alpha(0,t)^2 + \Big(\mu\lambda_1 - \frac{\mu}{2}\kappa_4\Big)\left|\tilde{Y}(t)\right|^2 \\
&+ \mu\frac{\lambda_1}{\xi_1}V(t) - \frac{\mu}{2}\eta m(t)\Big] \\
&- \frac{1}{\theta V(t) - \frac{\mu}{2}m(t)}\Big[-\theta\frac{\mu_0}{\xi_1}V(t) - \Big(\theta\lambda_{\alpha 1} - \frac{\mu}{2}\kappa_1\Big)\alpha(1,t)^2 \\
&- \Big(\theta\lambda_{\alpha 0} - \frac{\mu}{2}\kappa_2\Big)\alpha(0,t)^2 - \theta\lambda_{\alpha 0}d(t)^2 - \Big(\theta - \frac{\mu}{2}\kappa_4\Big)\left|\tilde{Y}(t)\right|^2 \\
&- \Big(\frac{\theta}{2\tau}r_c e^{-2} - \frac{\mu}{2}\kappa_3\Big)\hat{v}(2,t)^2 + \frac{\mu}{2}\eta m(t)\Big]\psi,
\end{aligned} \tag{140}$$

where $\Omega_1(t) \ge \Omega(t)$ has been used. Applying (120)–(122), (129) (the last four terms), and the following inequalities $-\frac{\frac{\mu}{2}\eta m(t)}{\theta V(t) - \frac{\mu}{2}m(t)} \le -\frac{\frac{\mu}{2}\eta m(t)}{-\frac{\mu}{2}m(t)} = \eta$, $\frac{V(t)}{\theta V(t) - \frac{\mu}{2}m(t)} \le \frac{V(t)}{\theta V(t)} = \frac{1}{\theta}$, $\frac{d(t)^2}{\theta V(t) - \frac{\mu}{2}m(t)} = \frac{d(t)^2 + \frac{\mu}{2}m(t) - \frac{\mu}{2}m(t)}{\theta V(t) - \frac{\mu}{2}m(t)} \le \psi(t) + 1$, which hold because of $m(t) < 0$, then (140) becomes

$$\begin{aligned}
\dot{\psi}(t) \le& \frac{(\frac{1}{\mu} + \mu\lambda_1)d(t)^2 + \mu\frac{\lambda_1}{\xi_1}V(t) - \frac{\mu}{2}\eta m(t)}{\theta V(t) - \frac{\mu}{2}m(t)} + \eta\psi \\
&+ \frac{\mu_0}{\xi_1}\psi + \theta\lambda_{\alpha 0}\psi^2 + \theta\lambda_{\alpha 0}\psi \\
\le& n_1\psi^2 + n_2\psi + n_3,
\end{aligned} \tag{141}$$

where $n_1 = \theta\lambda_{\alpha 0}$, $n_2 = \frac{1}{\mu} + \mu\lambda_1 + \eta + \mu_0 + \theta\lambda_{\alpha 0}$, $n_3 = \frac{1}{\mu} + \mu\lambda_1 + \frac{\mu\lambda_1}{\theta\xi_1} + \eta$ are positive constants. It follows that the time needed by ψ to go from 0 to 1 is at least

$$T = \int_0^1 \frac{1}{n_1 + n_2\bar{s} + n_3\bar{s}^2}d\bar{s} > 0 \tag{142}$$

which is independent of initial conditions. □

6. Stability analysis

In this section we state the main result of this paper, after we first establish an intermediate result.

Lemma 4. *With arbitrary initial data* $(\alpha(x,0), \beta(x,0))^T \in C^0([0,1];\mathbb{R}^2)$, $\hat{v}(x,0) \in C^1([1,2];\mathbb{R})$, $\hat{\zeta}(0) \in \mathbb{R}$, $m(0) \in \mathbb{R}^-$, *for* (101)–(106), (111), (117), *the exponential convergence is achieved in the sense of the norm* $|\hat{\zeta}(t)| + \|\alpha(\cdot,t)\| + \|\beta(\cdot,t)\| + \|\hat{v}(\cdot,t)\| + |m(t)|$.

Proof. Define

$$e(t) = \Upsilon_d e^{-\lambda_e t},$$

for some positive Υ_d, λ_e such that

$$\left|\tilde{Y}(t)\right| \le e(t), \tag{143}$$

recalling Theorem 1.

Let us consider the Lyapunov function

$$V_a(t) = V(t) - m(t) + \frac{1}{2}R_e e(t)^2 \tag{144}$$

where $m(t)$ is defined in (117) ($m(t) < 0$), and $V(t)$ is given in (119). By virtue of (139), we have that

$$d_1(\Omega_1(t) + |m(t)| + e(t)^2) \le V_a(t) \le d_2(\Omega_1(t) + |m(t)| + e(t)^2) \tag{145}$$

for some positive d_1, d_2. Taking the derivative of (144) along (101)–(106), (111), recalling (117), we obtain that

$$\begin{aligned}
\dot{V}_a(t) &= \dot{V} - \dot{m}(t) + R_e e(t)\dot{e}(t) \\
&= -a_{\rm m}\hat{\zeta}(t)^2 - \hat{\zeta}(t)b_1\alpha(1,t) + \frac{1}{2}q_2 e^{\delta_1}\beta(1,t)^2 - \frac{1}{2}q_2\beta(0,t)^2 \\
&- \frac{1}{2}\delta_1 q_2\int_0^1 e^{\delta_1 x}\beta(x,t)^2dx - g_4\int_0^1 e^{\delta_1 x}\beta(x,t)^2dx \\
&- \frac{1}{2}r_b q_1 e^{-\delta_2}\alpha(1,t)^2 + \frac{1}{2}q_1 r_b\alpha(0,t)^2 \\
&- \frac{1}{2}\delta_2 q_1 r_b\int_0^1 e^{-\delta_2 x}\alpha(x,t)^2dx - g_1 r_b\int_0^1 e^{-\delta_2 x}\alpha(x,t)^2dx \\
&- \frac{1}{2\tau}r_c\int_1^2 e^{-x}\hat{v}(x,t)^2dx - \frac{1}{2\tau}r_c e^{-2}\hat{v}(2,t)^2 \\
&+ \frac{1}{2\tau}r_c e^{-1}\hat{v}(1,t)^2 - R_e\lambda_e e(t)^2 + \eta m(t) + \kappa_1\alpha(1,t)^2 \\
&+ \kappa_2\alpha(0,t)^2 + \kappa_3\hat{v}(2,t)^2 + \kappa_4\left|\tilde{Y}(t)\right|^2.
\end{aligned} \tag{146}$$

Recalling (28), (115), (143), applying Young's inequality and the Cauchy–Schwarz inequality, we have

$$\begin{aligned}
\dot{V}_a(t) \le& -\frac{1}{2}\Big(a_{\rm m} - \frac{1}{\tau}r_c e^{-1}\Big)\hat{\zeta}(t)^2 \\
&- \Big(\frac{1}{2}q_1 r_b e^{-\delta_2} - \frac{q^2}{2}q_2 e^{\delta_1} - \frac{b_1^2}{2a_{\rm m}} - \kappa_1\Big)\alpha(1,t)^2 \\
&+ \Big(\frac{1}{2}q_1 r_b\lambda_d + \kappa_2\lambda_d\Big)\sup_{0\le\xi\le t} d(\xi)^2 \\
&- \Big(\frac{1}{2}\delta_1 q_2 - |g_4|\Big)\int_0^1 e^{\delta_1 x}\beta(x,t)^2dx \\
&- \Big(\frac{1}{2}\delta_2 q_1 r_b - r_b|g_1|\Big)\int_0^1 e^{-\delta_2 x}\alpha(x,t)^2dx \\
&- \frac{1}{2\tau}r_c\int_1^2 e^{-x}\hat{v}(x,t)^2dx - \Big(\frac{1}{2\tau}r_c e^{-2} - \kappa_3\Big)\hat{v}(2,t)^2 \\
&- (R_e\lambda_e - \kappa_4)e(t)^2 + \eta m(t).
\end{aligned} \tag{147}$$

Applying (123)–(127), and (132), we thus arrive at

$$\dot{V}_a(t) \le -\lambda_a V(t) + \eta m(t) - \kappa_4 e(t)^2 + \left(\frac{1}{2}q_1 r_b \lambda_d + \kappa_2 \lambda_d\right) \sup_{0\le\xi\le t} d(\xi)^2 \tag{148}$$

where λ_a is given in (131). Recalling (144), we have that

$$\dot{V}_a(t) \le -\sigma_a V_a(t) + \left(\frac{1}{2}q_1 r_b \lambda_d + \kappa_2 \lambda_d\right) \sup_{0\le\xi\le t} d(\xi)^2 \tag{149}$$

where σ_a is given in (130). Multiplying both sides of (149) by $e^{\sigma_a t}$, then applying integration from 0 to t, we have

$$V_a(t) \le V_a(0)e^{-\sigma_a t} + \frac{\lambda_d}{\sigma_a}(1 - e^{-\sigma_a t})\left(\frac{1}{2}q_1 r_b + \kappa_2\right) \sup_{0\le\xi\le t} d(\xi)^2$$
$$\le V_a(0)e^{-\sigma_a t} + \frac{\lambda_d}{\sigma_a}\left(\frac{1}{2}q_1 r_b + \kappa_2\right) \sup_{0\le\xi\le t} d(\xi)^2. \tag{150}$$

The triggering condition (116) guarantees

$$\sup_{0\le\xi\le t} d(\xi)^2 \le \theta \sup_{0\le\xi\le t} V(\xi) + \mu \sup_{0\le\xi\le t} |m(\xi)|. \tag{151}$$

Inserting (151) into (150), and then recalling (144), yields

$$V_a(t) \le V_a(0)e^{-\sigma_a t} + \frac{\lambda_d}{\sigma_a}\left(\frac{1}{2}q_1 r_b + \kappa_2\right) \times \sup_{0\le\xi\le t}(\theta V(\xi) + \mu|m(\xi)|)$$
$$\le V_a(0)e^{-\sigma_a t} + \bar{\Phi} \sup_{0\le\xi\le t} V_a(\xi), \tag{152}$$

where

$$\bar{\Phi} = \frac{\lambda_d}{\sigma_a}\left(\frac{1}{2}q_1 r_b + \kappa_2\right)\max\{\theta, \mu\}. \tag{153}$$

Recalling (128), (129) (the first term), we have that

$$\bar{\Phi} < 1. \tag{154}$$

The following estimate then holds

$$\sup_{0\le\xi\le t}\left(V_a(\xi)e^{\sigma_a\xi}\right) \le V_a(0) + \bar{\Phi} \sup_{0\le\xi\le t}\left(V_a(\xi)e^{\sigma_a\xi}\right)$$

as a consequence of (152). It follows that

$$\sup_{0\le\xi\le t} V_a(\xi) \le \Upsilon_V V_a(0)e^{-\sigma_a t} \tag{155}$$

where the constant

$$\Upsilon_V = \frac{1}{1-\bar{\Phi}} > 0 \tag{156}$$

by recalling (154). The choices of ETM parameters affect the overshoot coefficient in the exponential result according to (153), (156). Recalling (145), Lemma 4 is obtained. □

The block diagram of the output-feedback closed-loop system is shown in Fig. 2, where an observer-based continuous-in-time control signal $U(t)$ defined in (108), is updated at time instants t_k determined by ETM (116), (117) realized based on the observer (23)–(29), and between updates the control input signal is held constant in a zero-order-hold (ZOH) fashion. The well-posedness of the closed-loop system is ensured by Proposition 1 and Lemma 3.

The properties of the output-feedback closed-loop system are shown in the following theorem.

Theorem 2. *For all initial data* $(z(x,0), w(x,0))^T \in C^0([0,1],\mathbb{R}^2)$, $v(x,0) \in C^1([1,2],\mathbb{R})$, $\zeta(0) \in \mathbb{R}$, $(\hat{z}(x,0), \hat{w}(x,0))^T \in C^0([0,1],\mathbb{R}^2)$, $\hat{v}(x,0) \in C^1([1,2],\mathbb{R})$, $\hat{\zeta}(0) \in \mathbb{R}$, $m(0) \in \mathbb{R}^-$, *choosing the design parameters to satisfy (44), (107), (120)–(129), the output-feedback closed-loop system, i.e., the plant (14)–(19) under the event-based control input* $U_d(t)$ *in (109), which is realized using the observer (23)–(29), and the event-triggering mechanism (116), (117), has the following properties: (1) No Zeno phenomenon occurs, i.e.,* $\lim_{i\to\infty} t_i = +\infty$. *(2) The exponential convergence in the output-feedback event-based closed-loop system is achieved in the sense of the norm* $|\zeta(t)| + \|z(\cdot,t)\| + \|w(\cdot,t)\| + \|v(\cdot,t)\| + |\hat{\zeta}(t)| + \|\hat{z}(\cdot,t)\| + \|\hat{w}(\cdot,t)\| + \|\hat{v}(\cdot,t)\| + |m(t)|$. *(3) The event-triggered control input signal is convergent to zero in the sense of* $\lim_{t\to\infty} U_d(t) = 0$.

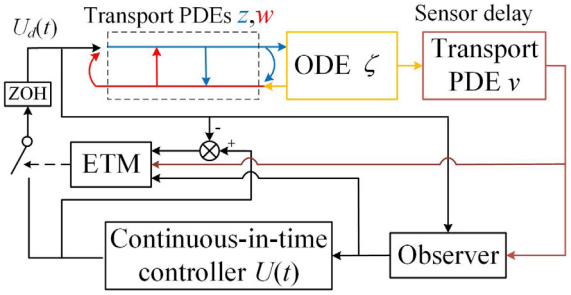

Fig. 2. Event-based closed-loop system.

Proof. (1) Recalling Lemma 3, we have that $t_i \ge iT$, $i \in \mathbb{Z}_+$. The property (1) is thus obtained.

(2) Through an additional analysis which is routine but heavy on additional notation, we know that the stability result in Lemma 4 still holds (by choosing a sufficiently large R_e) for the target system corresponding to the output-feedback loop, i.e., $\mathcal{S}$-system defined in Remark 1. Thus separation principle holds. Recalling the invertibility of the backstepping transformation (86), (87), and applying Theorem 1 as well as (31), the property (2) is thus obtained.

(3) Recalling (108) and the stability result proved in the property 2), we have that the continuous-in-time control input signal $U(t)$ is convergent to zero. According to the definition (109), the property (3) is obtained. □

7. Application in deep-sea construction

In the simulation, we consider the application of DCV to place equipment to be installed on the seabed for off-shore oil drilling. The equipment has to be installed accurately at the predetermined location with a tight tolerance, such as the permissible maximum tolerance of 2.5 m for a typical subsea installation, according to How et al. (2011). Applying the design presented above, an output-feedback control force employing piecewise-constant values at the crane is obtained, to reduce oscillations of the long cable and position the equipment in the target area, while compensating the sensor delay.

The DCV model in simulation is (14)–(19) with coefficients in (12), (13), whose values are shown in Table 1, and the obtained simulation results are represented in the $(\bar{z}, \bar{w})$ and u models which are on the spatial domain $[0, L]$ via (8), (9), (10), (11). The disturbances f, f_L, which will be formulated in next subsection, are included (with multiplying by $\frac{1}{\rho}$ considering the conversion from the wave PDE (1)–(4)) in the model (14)–(19). The initial conditions are chosen as $z(x,0) = 6\sin\left(5\pi x + \frac{\pi}{4}\right)$, $w(x,0) = 6\cos\left(5\pi x + \frac{\pi}{3}\right)$, which gives the ODE initial conditions $\zeta(0) = 3\sin\left(\frac{21\pi}{4}\right) + 3\cos\left(\frac{16\pi}{3}\right)$ by recalling (17), and the quantity is, physically, the initial oscillation velocity of the payload. According to the Riemann transformations (8), (9), and (10), (11), the initial

conditions of $\bar{z}$, $\bar{w}$ and the initial oscillation velocity of the cable are, hence, $\bar{z}(\bar{x},0)=6\sin\left(\frac{5\pi\bar{x}}{L}+\frac{\pi}{4}\right)$, $\bar{w}(\bar{x},0)=6\cos\left(\frac{5\pi\bar{x}}{L}+\frac{\pi}{3}\right)$, $u_t(\bar{x},0)=\frac{1}{2}(\bar{z}(\bar{x},0)+\bar{w}(\bar{x},0))$.

The initial distributed oscillation displacement of the cable is defined as $u(\bar{x},0)=0$, which, recalling (1), (3), implies that the initial displacement of the payload is $b_L(0)=0$. The initial values of the observer are defined as zero, i.e., $\hat{z}[0]=0$, $\hat{w}[0]=0$, $\hat{\zeta}(0)=0$, $\hat{v}[0]=0$. The initial value of the internal dynamic variable $m(t)$ in ETM is set as $m(0)=-1.5\times10^5$. The design parameters are chosen as $L_1=1$, $F_1=50$, $\kappa_1=3000$, $\kappa_2=\kappa_4=2000$, $\delta_1=0.017$, $\delta_2=0.01$, $r_c=0.2$, $r_b=40$, $\kappa_3=0.025$, $\mu=0.2$, $\theta=0.08$ according to (44), (107), (120)–(129), and the free design parameter η is picked as 8.

The oscillating drag forces $f(\bar{x},t)$ and $f_L(t)$, which are caused by ocean current disturbances, on the cable and the payload respectively, are modeled as (224), (225) in Wang and Krstic (2020b).

The numerical computation for the plant and observer is conducted using the finite difference method with the step sizes of t and x as 0.001, 0.05, respectively. The approximate solutions of the kernel PDEs used in the observer gains (45), (54), (57), (81), (85), and the control laws (108), (109), where the integral operators are approximated by sums, are also solved by the finite difference method based on discretization of the triangular domain into an uniformly spaced grid with the interval of 0.05. Notice that the derivatives in (70), (91), (96) are represented by a finite difference scheme in the direction of the information flow, i.e., along the line $x=y$, for the sake of avoiding using the points outside the triangular domain.

We concentrate on the end phase (20 s) of the descending process, i.e., when the payload is near the seabed and the cable is at the fully extended total length L. Our task is to reduce the oscillations of the cable and place the payload at the bottom of the cable in the target area on the seabed, namely, within the permissible tolerance of 2.5 m around the predetermined location (How et al., 2011), by applying a piecewise-constant control input at the onboard crane driving the top of the cable, where the measurements are transmitted from the seabed and subject to a 0.5 s delay, considering the transmission speed of acoustic signals in salty water is around 1500 m/s (Jiang, 2008; Manjula & Manvi, 2011).

The event-based control input defined in (109), and the continuous-in-time control input defined in (108), are shown in Fig. 3, where the number of triggering times is 15 and the minimal dwell time is 0.097 s. The control input is zero at the beginning due to the sensor delay and the zero initial conditions of the observer based on which the control law is realized. With the event-based control input, we know from Figs. 4, 5 that the PDE states $\bar{z}(\bar{x},t)$ and $\bar{w}(\bar{x},t)$ are regulated to a small range around zero, under the unknown ocean current disturbances f, f_L and the sensor delay $\tau=0.5$ s. Similar results of the observer errors $\tilde{z}(\bar{x},t)=\bar{z}(\bar{x},t)-\hat{z}(\frac{\bar{x}}{L},t)$, $\tilde{w}(\bar{x},t)=\bar{w}(\bar{x},t)-\hat{w}(\frac{\bar{x}}{L},t)$ are observed in Figs. 6, 7. Fig. 8 shows the internal dynamic variable $m(t)$ in ETM is less than zero all the time.

By virtue of (3), (6), the lateral displacement of the payload $b_L(t)$ is obtained as $b_L(t)=\int_0^t\zeta(\delta)d\delta+u(L,0)$. From Fig. 9, we know that the oscillation velocity of the payload, i.e., $\dot{b}_L(t)=\zeta(t)$, is convergent to zero, and the position error of the payload is -0.98 m from the desired location on the seabed, which satisfies the requirement of being within permissible tolerance of 2.5 m given in How et al. (2011). Moreover, compared with the delayed PD controller $U_{\rm pd}(t)=\frac{1}{c}(50\zeta(t-\tau)+2\dot{\zeta}(t-\tau))$ (the PD parameters are chosen by trial and error), whose performance on regulation of the payload is shown in Fig. 10 where the position error of the payload is -2.05 m, the proposed controller achieves the smaller position error, i.e., the equipment is installed at a

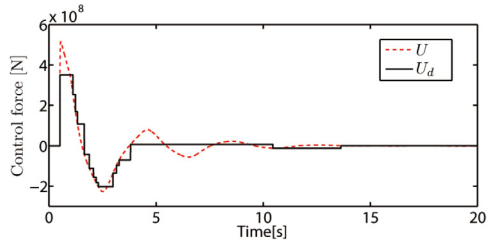

Fig. 3. Control forces.

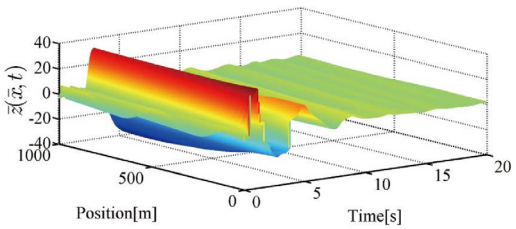

Fig. 4. The evolution of $\bar{z}(\bar{x},t)$ under the control input $U_d(t)$.

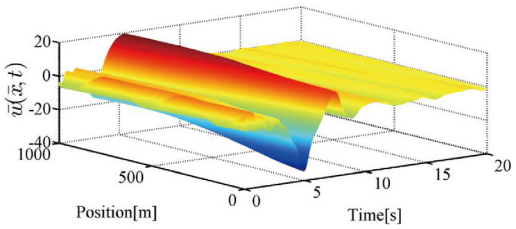

Fig. 5. The evolution of $\bar{w}(\bar{x},t)$ under the control input $U_d(t)$.

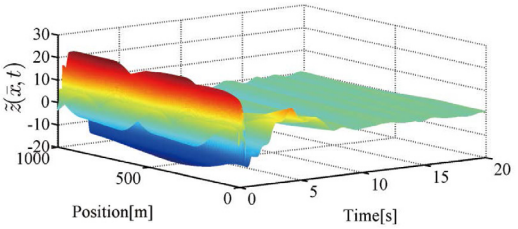

Fig. 6. The evolution of the observer error $\tilde{z}(\bar{x},t)$.

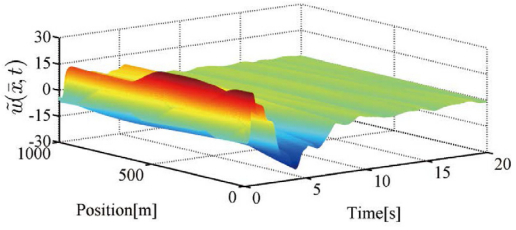

Fig. 7. The evolution of the observer error $\tilde{w}(\bar{x},t)$.

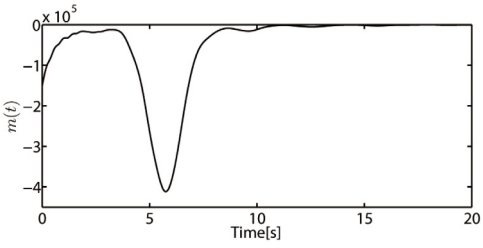

Fig. 8. The evolution of the internal dynamic variable $m(t)$ in ETM.

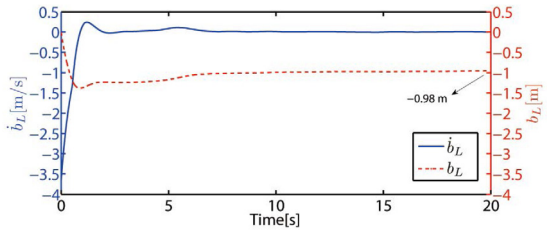

Fig. 9. The oscillation velocity and displacement of the payload under the proposed control input $U_d(t)$.

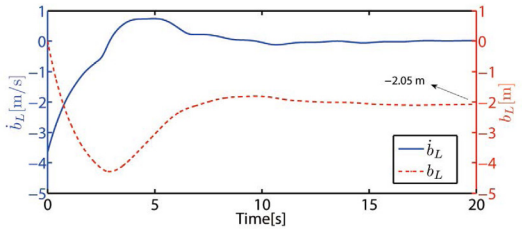

Fig. 10. The oscillation velocity and displacement of the payload under the traditional PD controller.

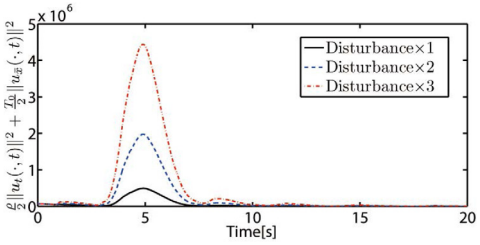

Fig. 11. The cable oscillation energy.

position closer to the target position. Through (8), (9), the cable lateral oscillation energy, including oscillation kinetic energy $\frac{\rho}{2}\|u_t(\cdot,t)\|^2$ and potential energy $\frac{T_0}{2}\|u_{\bar{x}}(\cdot,t)\|^2$, is represented by $z[t]$, $w[t]$ shown in Figs. 4, 5, as $\frac{\rho}{2}\|u_t(\cdot,t)\|^2+\frac{T_0}{2}\|u_x(\cdot,t)\|^2 = \frac{\rho}{8}\|w(\cdot,t)+z(\cdot,t)\|^2+\frac{\rho}{8}\|w(\cdot,t)-z(\cdot,t)\|^2$.

As shown in Fig. 11, the oscillation energy of the cable with the proposed control law is reduced to a low level after $t = 10$ s, under the external ocean current disturbances f, f_L. This result, the black line in Fig. 11, shows the robustness of the proposed controller to small disturbances. However, as we continue to increase the amplitude of the disturbance f, from the baseline value, to its twice, and to its triple, the results on cable oscillation energy are shown as the blue dash line and red dot dash line in Fig. 11, where performance deterioration of the proposed controller is observed with the increase of disturbance amplitudes, and relatively large vibrations appear at the triple disturbance.

8. Conclusion

We present the design of delay-compensated event-triggered boundary control for heterodirectional coupled hyperbolic PDE–ODE systems, where arbitrarily long delays existing in sensing are compensated and the control input employs piecewise-constant values. To this end, we treat the time delay as a transport PDE, followed by designing a "full-order" state observer for the overall system of heterodirectional coupled hyperbolic PDEs–ODE–transport PDE, only using the measurements at the right boundary of the last transport PDE. Then the delay-compensated event-triggered boundary controller is derived through a two-step design including an output-feedback continuous-in-time boundary stabilization law and the subsequent design of a dynamic event-triggering mechanism based on the evolution of the overall system. We prove the absence of a Zeno behavior and exponential convergence in the resulting event-based closed-loop system. In the simulation, the proposed design is applied in control of a deep-sea construction vessel, with using the piecewise-constant control input and compensating the sensor delays in communication between the seabed and the vessel on the ocean surface through a set of acoustics devices, to place the equipment to the target area on the seabed.

In the future work, the unknown delay, and generalization of the explicit design in Vazquez and Krstic (2014) by Marcum functions to PDE–ODE cascades will be considered. Moreover, disturbance rejection or adaptive cancellation methods will be incorporated in the control design to deal with the uncertain ocean current disturbances.

References

Aarsnes, U. J. F., Vazquez, R., Di Meglio, F., & Krstic, M. (2019). Delay robust control design of under-actuated PDE-ODE-PDE systems. In *American control conference* (pp. 3200–3205).

Ahmed-Ali, T., Karafyllis, I., & Lamnabhi-Lagarrigue, F. (2013). Global exponential sampled-data observers for nonlinear systems with delayed measurements. *Systems & Control Letters*, *62*, 539–549.

Auriol, J., Aarsnes, U. J. F., Martin, P., & Di Meglio, F. (2018). Delay-robust control design for two heterodirectional linear coupled hyperbolic PDEs. *IEEE Transactions on Automatic Control*, *63*(10), 3551–3557.

Auriol, J., Bribiesca-Argomedo, F., Saba, D. B., Di Loreto, M., & Di Meglio, F. (2018). Delay-robust stabilization of a hyperbolic PDE-ODE system. *Automatica*, *95*, 494–502.

Bin, M., & Di Meglio, F. (2016). Boundary estimation of boundary parameters for linear hyperbolic PDEs. *IEEE Transactions on Automatic Control*, *62*(8), 3890–3904.

Cacace, F., Germani, A., & Manes, C. (2010). An observer for a class of nonlinear systems with time varying observation delay. *Systems & Control Letters*, *59*(5), 305–312.

Coron, J. M., Vazquez, R., Krstic, M., & Bastin, G. (2013). Local exponential H^2 stabilization of a 2×2 quasilinear hyperbolic system using backstepping. *SIAM Journal on Control and Optimization*, *51*(3), 2005–2035.

Curtain, R., & Morris, K. (2009). Transfer functions of distributed parameter systems: A tutorial. *Automatica*, *45*, 1101–1116.

Deutscher, J., Gehring, N., & Kern, R. (2018). Output feedback control of general linear heterodirectional hyperbolic ODE-PDE-ODE systems. *Automatica*, *95*, 472–480.

Diagne, A., Diagne, M., Tang, S.-X., & Krstic, M. (2017). Backstepping stabilization of the linearized Saint-Venant-Exner model. *Automatica*, *76*, 345–354.

Diagne, M., & Karafyllis, I. (2021). Event-triggered control of a continuum model of highly re-entrant manufacturing system. *Automatica*, *134*, Article 109902.

Espitia, N. (2020). Observer-based event-triggered boundary control of a linear 2×2 hyperbolic systems. *Systems & Control Letters*, *138*, Article 104668.

Espitia, N., Girard, A., Marchand, N., & Prieur, C. (2016a). Event-based control of linear hyperbolic systems of conservation laws. *Automatica*, *70*, 275–287.

Espitia, N., Girard, A., Marchand, N., & Prieur, C. (2016b). Event-based stabilization of linear systems of conservation laws using a dynamic triggering condition. In *Proc. 10th IFAC symp. nonlinear control syst., Vol. 49* (pp. 362–367).

Espitia, N., Girard, A., Marchand, N., & Prieur, C. (2018). Event-based boundary control of a linear 2×2 hyperbolic system via backstepping approach. *IEEE Transactions on Automatic Control*, *63*(8), 2686–2693.

Espitia, N., Karafyllis, I., & Krstic, M. (2021). Event-triggered boundary control of constant-parameter reaction-diffusion PDEs: a small-gain approach. *Automatica*, *128*, Article 109562.

Germani, A., Manes, C., & Pepe, P. (2002). A new approach to state observation of nonlinear systems with delayed output. *IEEE Transactions on Automatic Control*, *47*(1), 96–101.

Girard, A. (2015). Dynamic triggering mechanisms for event-triggered control. *IEEE Transactions on Automatic Control*, *60*(7), 1992–1997.

Goatin, P. (2006). The Aw-Rascle vehicular traffic flow model with phase transitions. *Mathematical and Computer Modelling*, *44*, 287–303.

Guzman, P., Marx, S., & Cerpa, E. (2019). Stabilization of the linear Kuramoto-Sivashinsky equation with a delayed boundary control. *IFAC-PapersOnLine*, *52*(2), 70–75.

Hasan, A., Aama, O., & Krstic, M. (2016). Boundary observer design for hyperbolic PDE-ODE cascade systems. *Automatica*, *68*, 75–86.

He, W., & Ge, S. (2016). Cooperative control of a nonuniform gantry crane with constrained tension. *Automatica*, *66*, 146–154.
He, W., Meng, T., He, X., & Ge, S. (2018). Unified iterative learning control for flexible structures with input constraints. *Automatica*, *96*, 326–336.
Heemels, W. P. M. H., Johansson, K. H., & Tabuada, P. (2012). An introduction to event-triggered and self-triggered control. In *Proc. 51st IEEE conf. decis. control* (pp. 3270–3285).
How, B., Ge, S. S., & Choo, Y. S. (2010). Dynamic load positioning for subsea installation via adaptive neural control. *IEEE Journal of Oceanic Engineering*, *35*, 366–375.
How, B., Ge, S. S., & Choo, Y. S. (2011). Control of coupled vessel, crane, cable, and payload dynamics for subsea installation operations. *IEEE Transactions on Control Systems Technology*, *19*, 208–220.
Hu, L., Di Meglio, F., Vazquez, R., & Krstic, M. (2016). Control of homodirectional and general heterodirectional linear coupled hyperbolic PDEs. *IEEE Transactions on Automatic Control*, *61*(11), 3301–3314.
Jiang, Z. (2008). Underwater acoustic networks-issues and solutions. *International Journal of Intelligent Control and Systems*, *13*, 152–161.
Karafyllis, I., Espitia, N., & Krstic, M. (2021). Event-triggered gain scheduling of reaction-diffusion PDEs. *SIAM Journal on Control and Optimization*, *59*, 2047–2067.
Karafyllis, I., & Krstic, M. (2019). *Input-to-state stability for PDES*. Springer.
Koga, S., Bresch-Pietri, D., & Krstic, M. (2020). Delay compensated control of the Stefan problem and robustness to delay mismatch. *International Journal of Robust and Nonlinear*, *30*, 2304–2334.
Krstic, M. (2009a). Control of an unstable reaction-diffusion PDE with long input delay. *Systems & Control Letters*, *58*, 773–782.
Krstic, M. (2009b). *Delay compensation for nonlinear, adaptive, and PDE systems*. Springer.
Krstic, M. (2011). Dead-time compensation for wave/string PDEs. *Journal of Dynamic Systems, Measurement, and Control*, *133*(3), Article 031004.
Krstic, M., & Smyshlyaev, A. (2008). Backstepping boundary control for first-order hyperbolic PDEs and application to systems with actuator and sensor delays. *Systems & Control Letters*, *57*(9), 750–758.
Lhachemi, H., & Prieur, C. (2020). Feedback stabilization of a class of diagonal infinite-dimensional systems with delay boundary control. *IEEE Transactions on Automatic Control*, *66*(1), 105–120.
Lhachemi, H., Prieur, C., & Shorten, R. (2019). An LMI condition for the robustness of constant-delay linear predictor feedback with respect to uncertain time-varying input delays. *Automatica*, *109*, Article 108551.
Manjula, R. B., & Manvi, S. S. (2011). Issues in underwater acoustic sensor networks. *International Journal of Electrical and Computer Engineering*, *3*(1), 101–110.
Marchand, N., Durand, S., & Castellanos, J. F. G. (2013). A general formula for event-based stabilization of nonlinear systems. *IEEE Transactions on Automatic Control*, *58*(5), 1332–1337.
Meglio, F. D., Bribiesca, F., Hu, L., & Krstic, M. (2018). Stabilization of coupled linear heterodirectional hyperbolic PDE-ODE systems. *Automatica*, *87*, 281–289.
Meglio, F. D., Lamare, P.-O., & Aarsnes, U. J. F. (2020). Robust output feedback stabilization of an ODE-PDE-ODE interconnection. *Automatica*, *119*, Article 109059.
Prieur, C., & Trelat, E. (2018). Feedback stabilization of a 1-D linear reaction-diffusion equation with delay boundary control. *IEEE Transactions on Automatic Control*, *64*(4), 1415–1425.
Prieur, C., & Winkin, J. (2018). Boundary feedback control of linear hyperbolic systems: application to the Saint-Venant-Exner equations. *Automatica*, *89*, 44–51.
Saba, D. B., Bribiesca-Argomedo, F., Loreto, M. D., & Eberard, D. (2019). Strictly proper control design for the stabilization of 2×2 linear hyperbolic ODE-PDE-ODE systems. In *58th IEEE conf. decis. control* (pp. 4996–5001).
Selivanov, A., & Fridman, E. (2016). Distributed event-triggered control of diffusion semilinear PDEs. *Automatica*, *68*, 344–351.
Seuret, A., Prieur, C., & Marchand, N. (2014). Stability of non-linear systems by means of event-triggered sampling algorithms. *IMA Journal of Mathematical Control and Information*, *31*(3), 415–433.
Stensgaard, T., White, C., & Schiffer, K. (2010). Subsea hardware installation from a FDPSO. In *Offshore technology conference*.
Tabuada, P. (2007). Event-triggered real-time scheduling of stabilizing control tasks. *IEEE Transactions on Automatic Control*, *52*, 1680–1685.
Vazquez, R., & Krstic, M. (2014). Marcum Q-functions and explicit kernels for stabilization of 2×2 linear hyperbolic systems with constant coefficients. *Systems & Control Letters*, *68*, 33–42.
Vazquez, R., Krstic, M., & Coron, J. M. (2011). Backstepping boundary stabilization and state estimation of a 2×2 linear hyperbolic system. In *50th IEEE conf. decis. control eur. control conf.* (pp. 4937–4942).
Wang, J., Koga, S., Pi, Y., & Krstic, M. (2018). Axial vibration suppression in a PDE model of ascending mining cable elevator. *Journal of Dynamic Systems, Measurement, and Control*, *140*, Article 111003.
Wang, J., & Krstic, M. (2020a). Delay-compensated control of sandwiched ODE-PDE-ODE hyperbolic systems for oil drilling and disaster relief. *Automatica*, *120*, Article 109131.
Wang, J., & Krstic, M. (2020b). (Supplementary document) Delay-compensated control of sandwiched ODE-PDE-ODE hyperbolic systems for oil drilling and disaster relief. arXiv preprint, arXiv:1910.05948.
Wang, J., & Krstic, M. (2021a). Adaptive event-triggered PDE control for load-moving cable systems. *Automatica*, *129*, Article 109637.
Wang, J., & Krstic, M. (2021c). Regulation-triggered adaptive control of a hyperbolic PDE-ODE model with boundary interconnections. *International Journal of Adaptive Control and Signal Processing*, *35*(8), 1513–1543.
Wang, J., & Krstic, M. (2021d). Vibration suppression for coupled wave PDEs in deep-sea construction. *IEEE Transactions on Control Systems Technology*, *29*(4), 1733–1749.
Wang, J., & Krstic, M. (2022). Event-triggered output-feedback backstepping control of sandwiched hyperbolic PDE systems. *IEEE Transactions on Automatic Control*, *67*(1), 220–235.
Wang, J., Krstic, M., & Pi, Y. (2018). Control of a 2×2 coupled linear hyperbolic system sandwiched between two ODEs. *International Journal of Robust and Nonlinear*, *28*, 3987–4016.
Yao, Z., & El-Farra, N. H. (2013). Resource-aware model predictive control of spatially distributed processes using event-triggered communication. In *52nd IEEE conf. decis. control* (pp. 3726–3731).
Yu, H., & Krstic, M. (2019). Traffic congestion control for Aw-Rascle-Zhang model. *Automatica*, *100*, 38–51.

Ji Wang received the Ph.D. degree in Mechanical Engineering in 2018 from Chongqing University, Chongqing, China. From 2019 to 2021, He was a postdoctoral scholar in the Department of Mechanical and Aerospace Engineering at University of California, San Diego, La Jolla, CA, USA. He is currently an associate professor in the Department of Automation at Xiamen University, Xiamen, China. Since 2021, he serves as Associate Editor of Systems & Control Letters. His research interests include modeling and control of distributed parameter systems, active disturbance rejection control, event-triggered control, and adaptive control, with applications in cable-driven mechanisms.

Miroslav Krstic is Distinguished Professor of Mechanical and Aerospace Engineering, holds the Alspach endowed chair, and is the founding director of the Cymer Center for Control Systems and Dynamics at UC San Diego. He also serves as Senior Associate Vice Chancellor for Research at UCSD. As a graduate student, Krstic won the UC Santa Barbara best dissertation award and student best paper awards at CDC and ACC. Krstic has been elected Fellow of seven scientific societies – IEEE, IFAC, ASME, SIAM, AAAS, IET (UK), and AIAA (Assoc. Fellow) – and as a foreign member of the Serbian Academy of Sciences and Arts and of the Academy of Engineering of Serbia. He has received the Richard E. Bellman Control Heritage Award, SIAM Reid Prize, ASME Oldenburger Medal, Nyquist Lecture Prize, Paynter Outstanding Investigator Award, Ragazzini Education Award, IFAC Nonlinear Control Systems Award, Chestnut textbook prize, Control Systems Society Distinguished Member Award, the PECASE, NSF Career, and ONR Young Investigator awards, the Schuck ('96 and '19) and Axelby paper prizes, and the first UCSD Research Award given to an engineer. Krstic has also been awarded the Springer Visiting Professorship at UC Berkeley, the Distinguished Visiting Fellowship of the Royal Academy of Engineering, the Invitation Fellowship of the Japan Society for the Promotion of Science, and four honorary professorships outside of the United States. He serves as Editor-in-Chief of Systems & Control Letters and has been serving as Senior Editor in Automatica and IEEE Transactions on Automatic Control, as editor of two Springer book series, and has served as Vice President for Technical Activities of the IEEE Control Systems Society and as chair of the IEEE CSS Fellow Committee. Krstic has coauthored fifteen books on adaptive, nonlinear, and stochastic control, extremum seeking, control of PDE systems including turbulent flows, and control of delay systems.